

The source of the Canary current in fall 2009

M. Dolores Pérez-Hernández,¹ Alonso Hernández-Guerra,¹ Eugenio Fraile-Nuez,² Isis Comas-Rodríguez,¹ Verónica M. Benítez-Barrios,² J. Francisco Domínguez-Yanes,² Pedro Vélez-Belchí,² and Demetrio De Armas²

Received 21 November 2012; revised 29 April 2013; accepted 30 April 2013; published 11 June 2013.

[1] The source of the Canary Current has been inferred from an inverse box model applied to the hydrographic data of a survey carried out in 2009 in the northeast subtropical gyre (29–37°N, 9–24°W). The Portugal Current is observed between 13.5 and 14.8°W at 37°N carrying 1.8 ± 0.4 Sv southward. This current presumably merges with the eastward transport of the Azores Current System and partly contributes to the Mediterranean inflow and partly to the northward recirculation of the Azores Current through the Gulf of Cadiz. The Azores Current System is located in the meridional range 33.50–36.25°N at 24.50°W. This System transports eastward 7.2 ± 0.5 Sv in the thermocline layers and 1.1 ± 0.8 Sv at intermediate layers. The Azores Current intermediate water mass has the highest portion of Sub-Arctic intermediate water (SAIW) in the region, while the Azores Countercurrent intermediate waters mass is mainly Mediterranean water. The Canary Current extends from 22.25° to 18.50°W at 29°N, the westernmost position ever observed. This current transports southward -6.2 ± 0.6 Sv in the thermocline layers and -2.0 ± 0.8 Sv in the intermediate layers. This intermediate flow shows a relative maximum of oxygen and a relative minimum in nutrient concentration, indicating the presence of SAIW. The study concludes that, at least in fall 2009, the Canary Current extends to the intermediate waters ($\gamma_n \leq 27.9220$ approximately 1600 dbar) and that Azores Current feeds the Canary Current at surface and intermediate layers.

Citation: Pérez-Hernández, D. M., A. Hernández-Guerra, E. Fraile-Nuez, I. Comas-Rodríguez, V. M. Benítez-Barrios, J. F. Domínguez-Yanes, P. Vélez-Belchí and D. De Armas (2013), The source of the Canary current in fall 2009, *J. Geophys. Res. Oceans*, 118, 2874–2891, doi:10.1002/jgrc.20227.

1. Introduction

[2] The Canary Current is the eastern boundary of the North Atlantic subtropical gyre that flows through the Canary Islands Archipelago. The study of the Canary Current first began by using historical data [Stramma, 1984; Stramma and Isemer, 1988; Stramma and Siedler, 1988], and has been studied with *in situ* data in the recent years [Hernández-Guerra *et al.*, 2002; Pelegrí *et al.*, 2005; Machín *et al.*, 2006; Fraile-Nuez *et al.*, 2010]. The ocean circulation maps prior to the 1980s show a Canary Current being fed by the Portugal Current. This current is a southward flow close to the coast of Portugal that is fed by a branch of the North Atlantic Current. This view changed after the studies by Krauss and Wuebbler [1982], Stramma

[1984], and Stramma and Siedler [1988]. These studies point out that the source of the Canary Current is an eastward branch of the Azores Current that was first described by Klein and Siedler [1989]. Although several authors still suggest that the Portugal Current also feeds the Canary current [Paillet and Mercier, 1997; Tomczak and Godfrey, 2003].

[3] The Canary Current carries an average of -3.0 ± 1.0 Sv ($1\text{Sv} = 10^6\text{m}^3\text{s}^{-1} \simeq 10^9\text{kg s}^{-1}$) to the south [Machín *et al.*, 2006]. These authors, using data from one cruise from each season and applying an inverse box model, describe the seasonal variability of the Canary Current. Their results show a Canary Current that presents a seasonal change in location and magnitude: it flows near the African coast in spring (2.8 ± 1.2 Sv), through the entire archipelago in summer (2.9 ± 1.1 Sv), only through the western islands in fall (4.5 ± 1.2 Sv) and is almost negligible in winter (1.7 ± 1.0 Sv). This behavior was also observed in Mason *et al.* [2011] using a Regional Ocean Modeling System model in the Canary region.

[4] In Käse and Siedler [1982], the Azores Current is defined as an eastward flow of 10 Sv and 60 km wide. This study suggests that the Azores Current is an extension of the North Atlantic Current, that was later confirmed by Stramma [1984] and Gould [1985]. The current presents a seasonal

¹Instituto de Oceanografía y Cambio Global, Universidad de Las Palmas de Gran Canaria, Las Palmas, Spain.

²Centro Oceanográfico de Canarias, Instituto Español de Oceanografía, Santa Cruz de Tenerife, Spain.

Corresponding author: M. D. Pérez-Hernández, Instituto de Oceanografía y Cambio Global, Universidad de Las Palmas de Gran Canaria, Las Palmas 35017, Spain. (maria.perez263@alu.ulpgc.es)

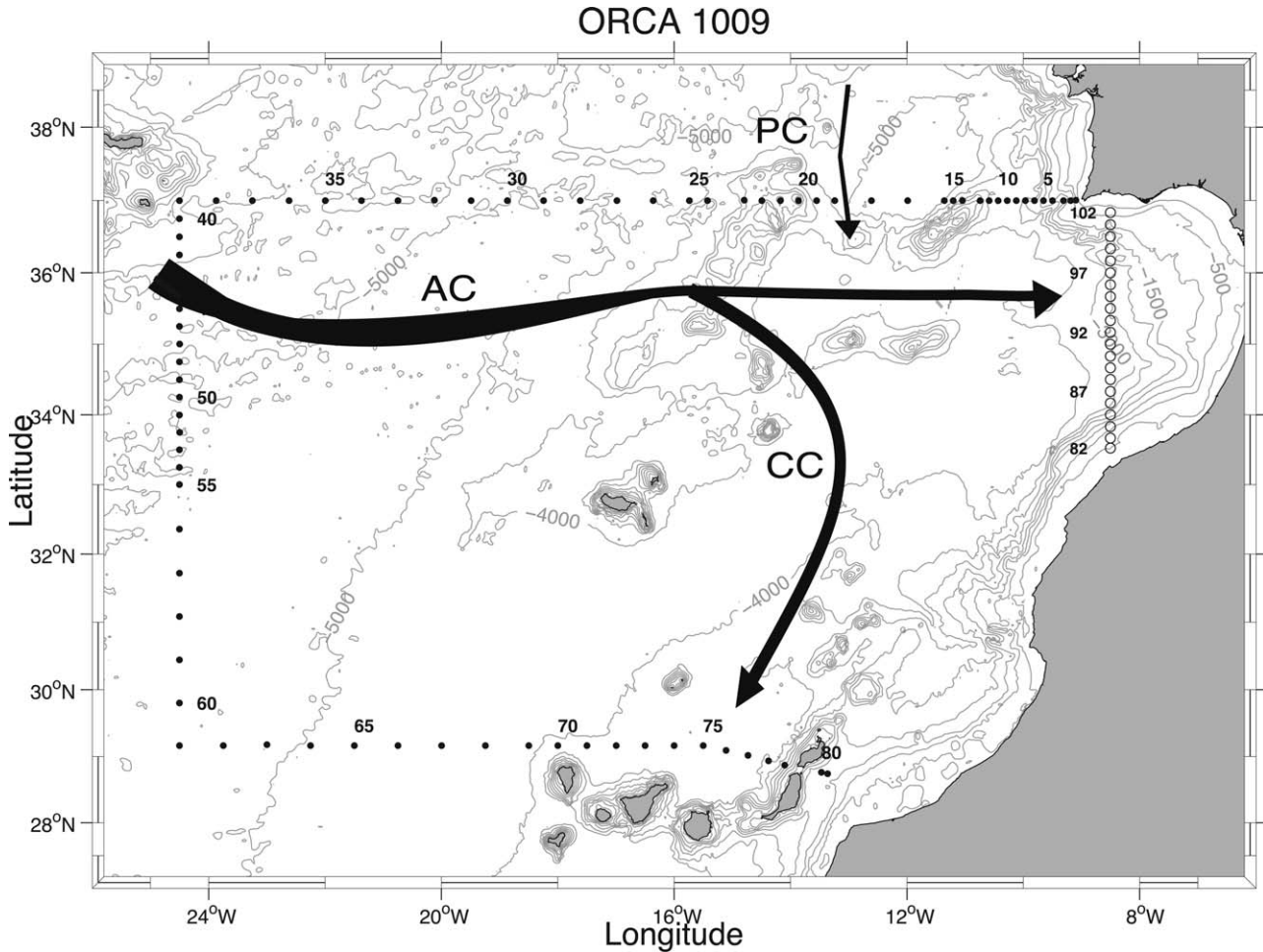


Figure 1. Geographical location of the stations, in which data was used in this study. Black dots correspond to the ORCA 1009 stations and white dots are those of AR06_1992. The arrows represent the currents in the study region, AC, PC, and CC stand for Azores Current, Portugal Current, and Canary Current, respectively.

variability, being in the range of 7–14 Sv [Arhan *et al.*, 1994; Alves *et al.*, 2002]. The Azores Current has an associated westward flow called the Azores Countercurrent.

[5] The Azores Countercurrent was first hypothesized in Onken [1993], although a westward flow had already been observed in Stramma and Müller [1989]. This countercurrent transports 2–7 Sv [Fiekas *et al.*, 1992; Kida *et al.*, 2008; Comas-Rodríguez *et al.*, 2011] which reduces the net eastward transport. The Azores Current, together with the Azores Countercurrent, forms the Azores Current System [Alves, 1996; Barbosa *et al.*, 2011].

[6] The aim of this study is to estimate circulation in the northeast subtropical gyre and to infer the source and mass transport of the Canary Current in fall 2009. For this purpose an inverse box model and water mass determination is applied to the Origen de la Corriente de Canarias (ORCA) cruise carried out in the region in fall 2009. First, we will present the data used in this study (section 2). In section 3, we will proceed to describe the different water masses in the region and their location. In section 4, the estimated initial geostrophic transport will be analyzed. The inverse box model will be described in section 5 and the estimated

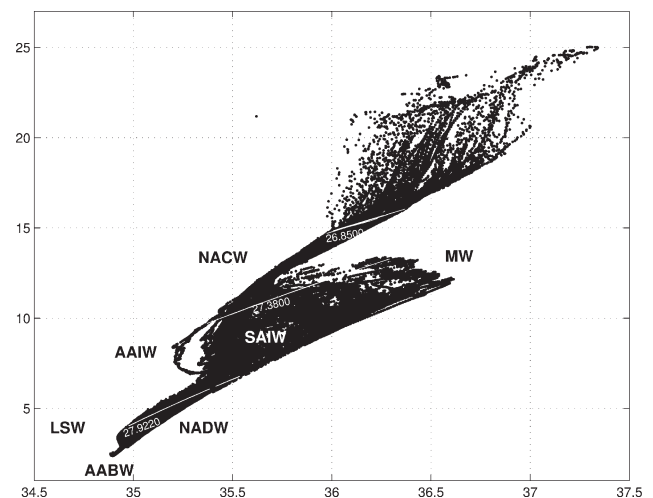


Figure 2. Potential temperature/salinity diagram for all stations. Plotted isopycnals (gray lines) are $\gamma_n = 26.8500$, 27.3800 , and $27.9220 \text{ kg m}^{-3}$ which roughly divides the water column into central, intermediate and bottom waters.

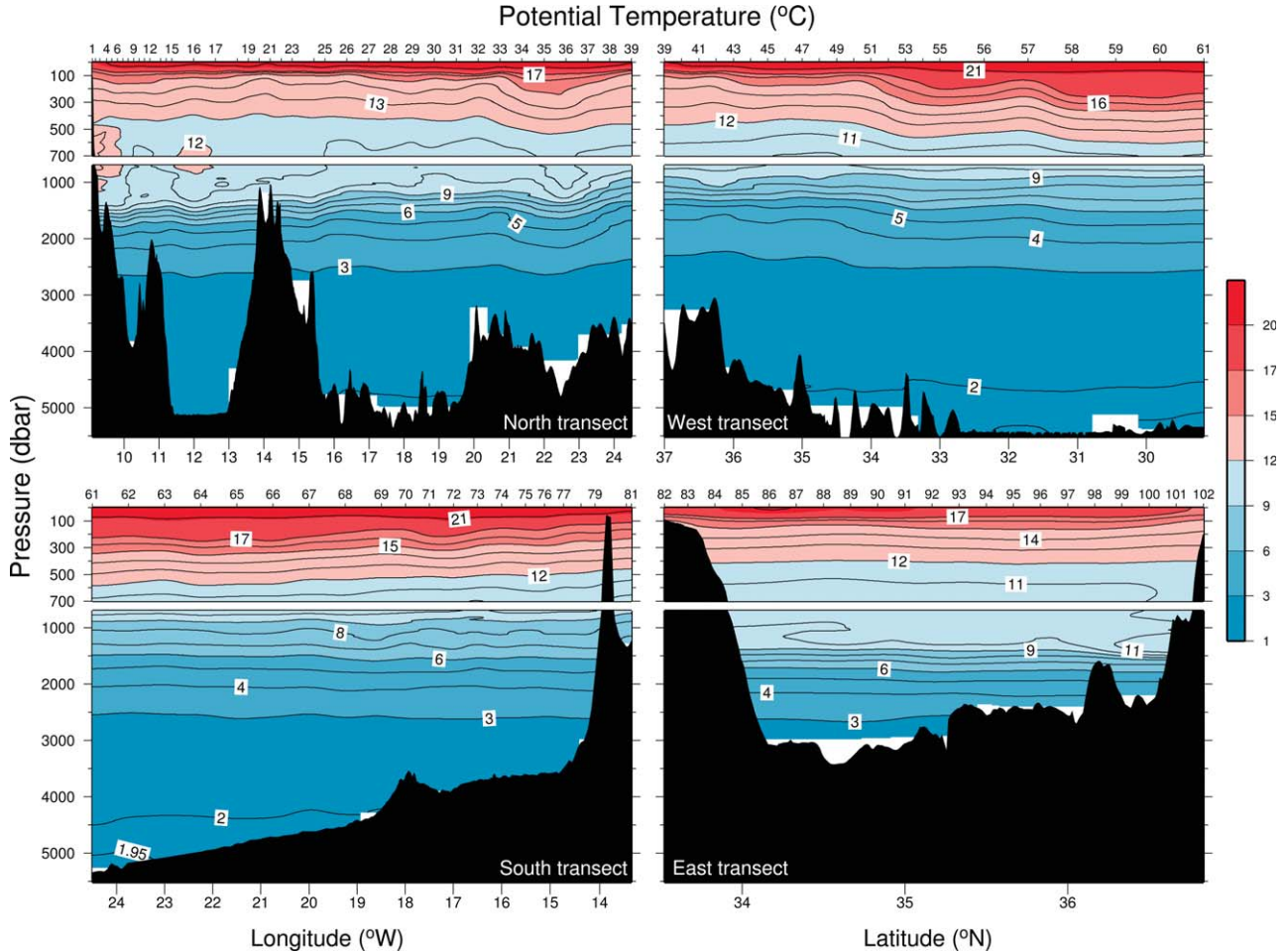


Figure 3. Vertical sections of potential temperature for the (upper-left corner) northern, (upper-right corner) western, (lower-left corner) southern, and (lower-right corner) eastern sections.

adjusted mass transport will be shown in section 6. Finally, we will discuss and conclude our results in section 7.

2. Data

[7] A total of 81 Sea bird 911 + conductivity-temperature-depth (CTD) stations closing the easternmost end of the Azores Current and the Canary Current are used (Figure 1, black dots). The box, covering the region 28.7–37.0°N and 9.1–24.5°W, was carried out between 15 October and 11 November 2009 onboard the BIO Hespérides. The northern, western and southern sections have 39, 22, and 21 stations, respectively. The CTD was equipped with redundant temperature and conductivity sensors.

[8] Water samples were collected at each station with a 24–10 L bottle carousel in order to estimate dissolved oxygen, nitrates, phosphates and silicates, and also to calibrate the CTD conductivity sensor. Conductivity was calibrated using a Guildline AUTOSAL model 8400B salinometer with a precision better than 0.002 for single samples. Dissolved oxygen was measured by *Winkler* [1888] oxygen determination using *Carpenter* [1965a, 1965b] and *Carritt and Carpenter* [1966] modifications. Because of instrument

problems, dissolved oxygen at stations 8, 21, and 59 were not obtained.

[9] For nutrients, water samples of 15 ml were collected in stoppered polypropylene conical centrifuge tubes. Samples for analysis were fitted directly onto the AutoSampler of a four channels Technicon-Bran Luebbe AA II AutoAnalyzer for determination by continuous flow analysis using methodology described in *Tréguer and Le Corre* [1975] for nitrates, *Flokard* [1978] for silicates, and *Zimmermann et al.* [1997] for phosphates. Data from stations 8 and 59 were not available.

[10] To close the box needed for the inverse model, temperature and salinity data from World Ocean Circulation Experiment (WOCE), AR06_1992 (http://cchdo.ucsd.edu/data_access/show_cruise?ExpoCode=07AL692_1) cruise have been used to determine the mass transport exchange per layer, between the Atlantic Ocean and the Mediterranean Sea. This meridional section was done during September 1992 and consisted of eight different sections. We only use the section that crosses the Strait of Gibraltar. This section consists of 21 stations at 8.5°W from 33.5 to 36.8°N (Figure 1, white dots). Due to data noise, a running filter was applied to smooth the temperature and salinity profiles. It is worth mentioning that the obtained transports for this cruise are within the ranges of inflow and outflow of 0.9–1.1 and 0.8–1.1 Sv described in *Candela* [2001].

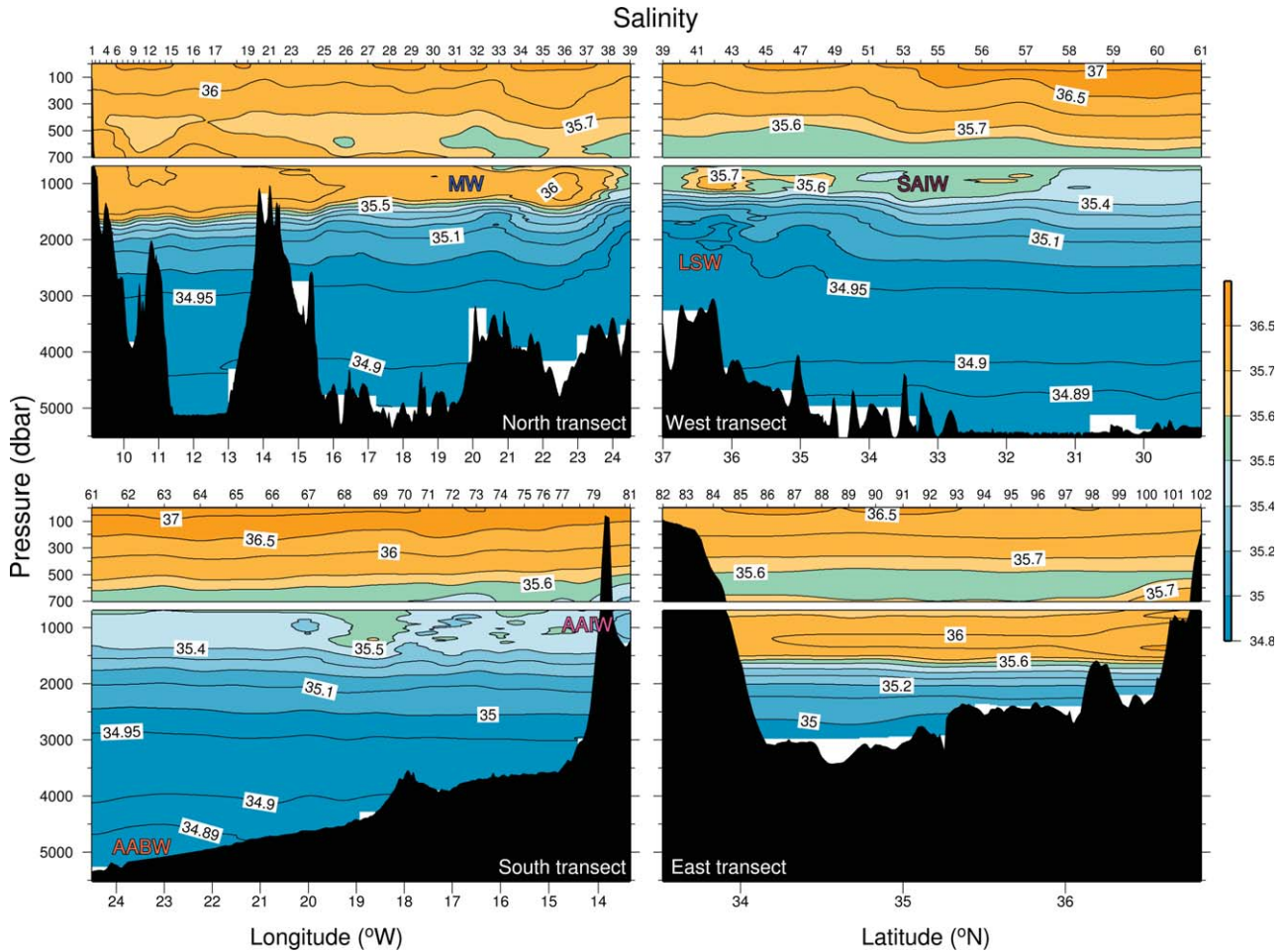


Figure 4. Vertical sections of salinity for the presence of the (upper-left corner) northern, (upper-right corner) western, (lower-left corner) southern, and (lower-right corner) eastern sections. The presence of the main water masses is indicated.

[11] Winds from the National Centers for Environmental Prediction (NCEP) reanalysis project from the National Oceanic and Atmospheric Administration (February 2011, <http://www.esrl.noaa.gov/psd/data/reanalysis/reanalysis.shtml>) together with scatterometer QuikScat (QS) winds (<http://coaps.fsu.edu/scatterometry/downloads/form.php>) are used to estimate the initial Ekman transport and uncertainties in each transect. Da Silva atlas of surface marine data 1994 (SMD94) (<http://iridl.ldeo.columbia.edu/SOURCES/.DASILVA/SMD94/>) database was used to estimate the evaporation-precipitation rate in order to have the initial value of freshwater flux for the inverse model.

3. Hydrography and Water Masses Characterization

[12] Waters above the seasonal thermocline are shown in Figures 2 and 5 with $\gamma_n < 26.8500 \text{ kg m}^{-3}$. They have scattered temperature and salinity values due to seasonal heating and evaporation. These waters occupy the region from the surface to 100–300 dbar (Figures 3 and 4, their lower limit is marked by the isolines 17°C and 36.5, respectively).

[13] The central water mass of the region appears between $10 < \theta < 17^\circ\text{C}$ and $35.6 < S < 36.7$ (Figures 2–4). Following Harvey [1982], Tomczak and Godfrey [2003], and Emery [2003], this water mass is North Atlantic central water (NACW). It extends to $\gamma_n \approx 27.3800 \text{ kg m}^{-3}$ coinciding with the end of the permanent thermocline (Figures 2 and 5) [Hernández-Guerra et al., 2005; Machín et al., 2006]. In Figure 5, the north transect presents a high-mesoscale signal. The west transects shows a negative slope of isoneutrals that reaches to the intermediate layers, indicating the presence of a net eastward flow and it is clearly observed mesoscale activity. This negative slope coincides with the deepening of the 17°C isotherm and the 36–36.5 isohalines (around station 52), characteristic of the Azores Front [Pérez et al., 2003; Comas-Rodríguez et al., 2011]. Along the south transect, isoneutrals at the permanent thermocline present a positive slope to the African shelf, resulting in a southward flow. Observed oxygen values of NACW are quite similar to the north section of Hernández-Guerra et al. [2005] (Figure 6). Nitrate and phosphate values of NACW are $6\text{--}17 \mu\text{mol kg}^{-1}$ and $0.30\text{--}1.11 \mu\text{mol kg}^{-1}$ respectively, which agree with the values in Pérez et al. [1993] at the Iberian

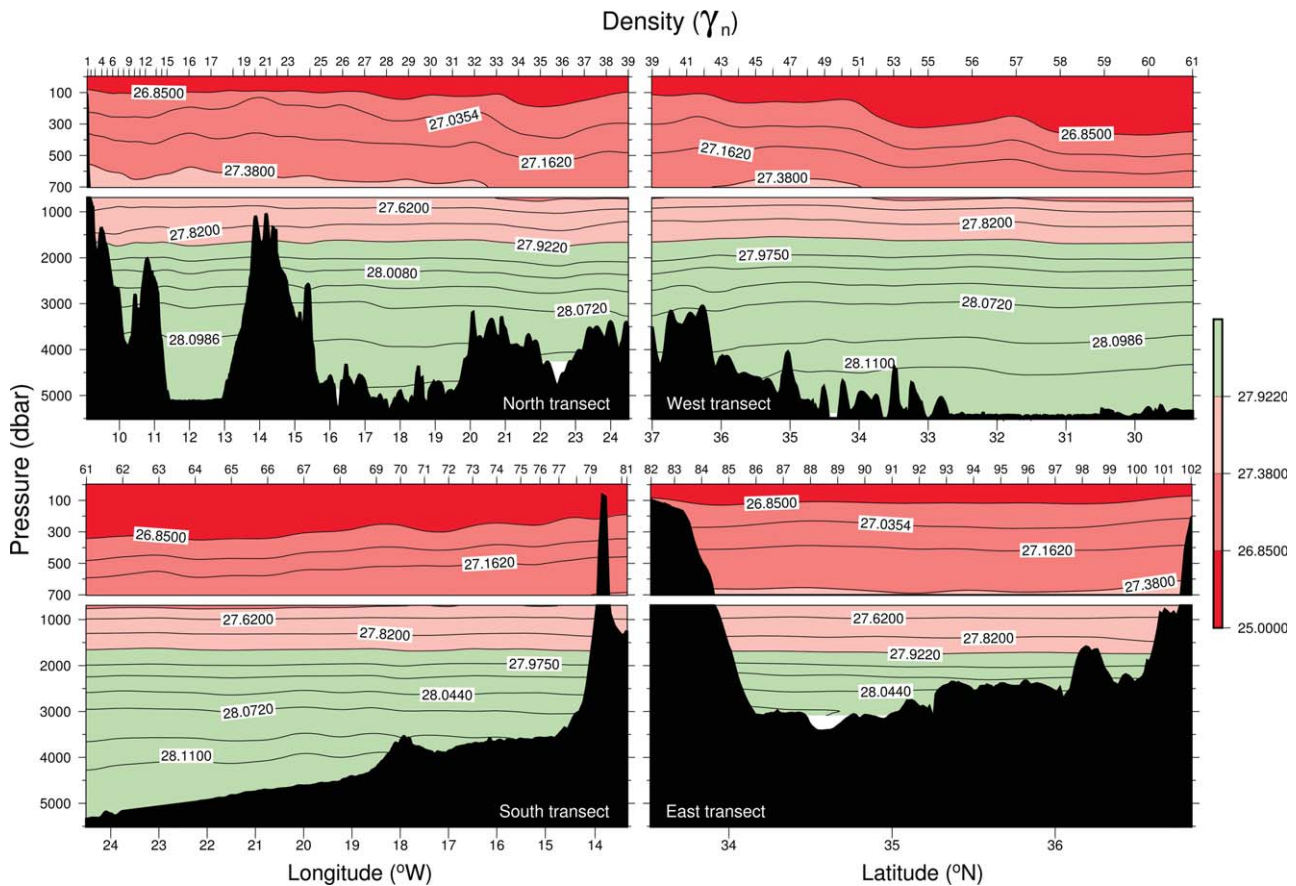


Figure 5. Vertical sections of neutral density for the northern (upper-left corner), western (upper-right corner), southern (lower-left corner), and eastern (lower-right corner) sections.

Peninsula (Figures 7 and 8). Silicates are between 0.6 and $6.0 \mu\text{mol kg}^{-1}$, also in agreement with Pérez *et al.* [1993] (Figure 9).

[14] Three intermediate water masses are found in the range $27.3800 < \gamma_n < 27.9220 \text{ kg m}^{-3}$ in the θ/S diagram (Figure 2): Mediterranean water (MW) with its characteristic high temperatures and salinities, Antarctic intermediate water (AAIW) with the lowest intermediate salinity values, and some contribution of sub-Arctic intermediate water (SAIW) in between. As seen in Table 1, the intermediate water masses of the region show a considerable overlap between them that allows diapycnal and isopycnal mixing. To discern between them, an O_2/S diagram together with the mixing triangle method is applied at $\gamma_n \sim 27.8000 \text{ kg m}^{-3}$ (ca.1255 dbar) (Figure 10). The triangle is defined by the values of pure MW from Van Aken [2000b], SAIW from Harvey and Arhan [1988], and AAIW from Cabeçadas *et al.* [2003]. This figure reveals that all the intermediate waters of the region contain a relevant content of MW. The high-salinity values near the MW vertex correspond to the stations located near Cape San Vicente (northeast corner of the region). The values outside of the mixing triangle, with higher oxygen and salinities than Van Aken's [2000b] values, are from the north stations nearest to the Iberian coast, where a core of MW can be seen (Figures 3 and 4). From east to west, the north transect decreases its content of MW. In the west transect, MW is

only seen forming a patch north of the Azores Front (Figure 4, stations 40–45), where the neutral density section shows a slight positive slope to the south, indicating that the MW is flowing west. As in Arhan *et al.* [1994], those intermediate waters with a high content of MW have oxygen values of ca. $190 \mu\text{mol kg}^{-1}$ and nitrates about $17 \mu\text{mol kg}^{-1}$ (this value also agrees with Castro *et al.* [1998]) (Figures 6 and 7). Phosphate values are in the range $0.90\text{--}1.20 \mu\text{mol kg}^{-1}$, which is quite similar to the ones obtained by Pérez *et al.* [1993] and Castro *et al.* [1998] (Figure 8). Silicate values for MW are ca. $8 \mu\text{mol kg}^{-1}$ agree with Van Aken [2000b] (Figure 9).

[15] Waters with the biggest content of SAIW in the study area occupy the northwest corner (stations 38–40) and most of the west transect (stations 45–57). In the O_2/S diagram, this water appears with lower salinities than the MW and high oxygen values (Figure 10). This intermediate water with high content of SAIW is responsible for the decrease in temperature and salinity between stations 38 and 57 (Figures 3 and 4). South of the Azores Front, isoneutrals between stations present a negative slope to the south, showing an eastward flow (Figure 5). A front in salinity is observed at station 58, indicating the presence of an adjacent water mass (Figure 4 west transect and Figure 10 dots and black asterisks). The front between both water masses is revealed in all vertical sections as a contrast of high/low salinities and oxygen values and low/high

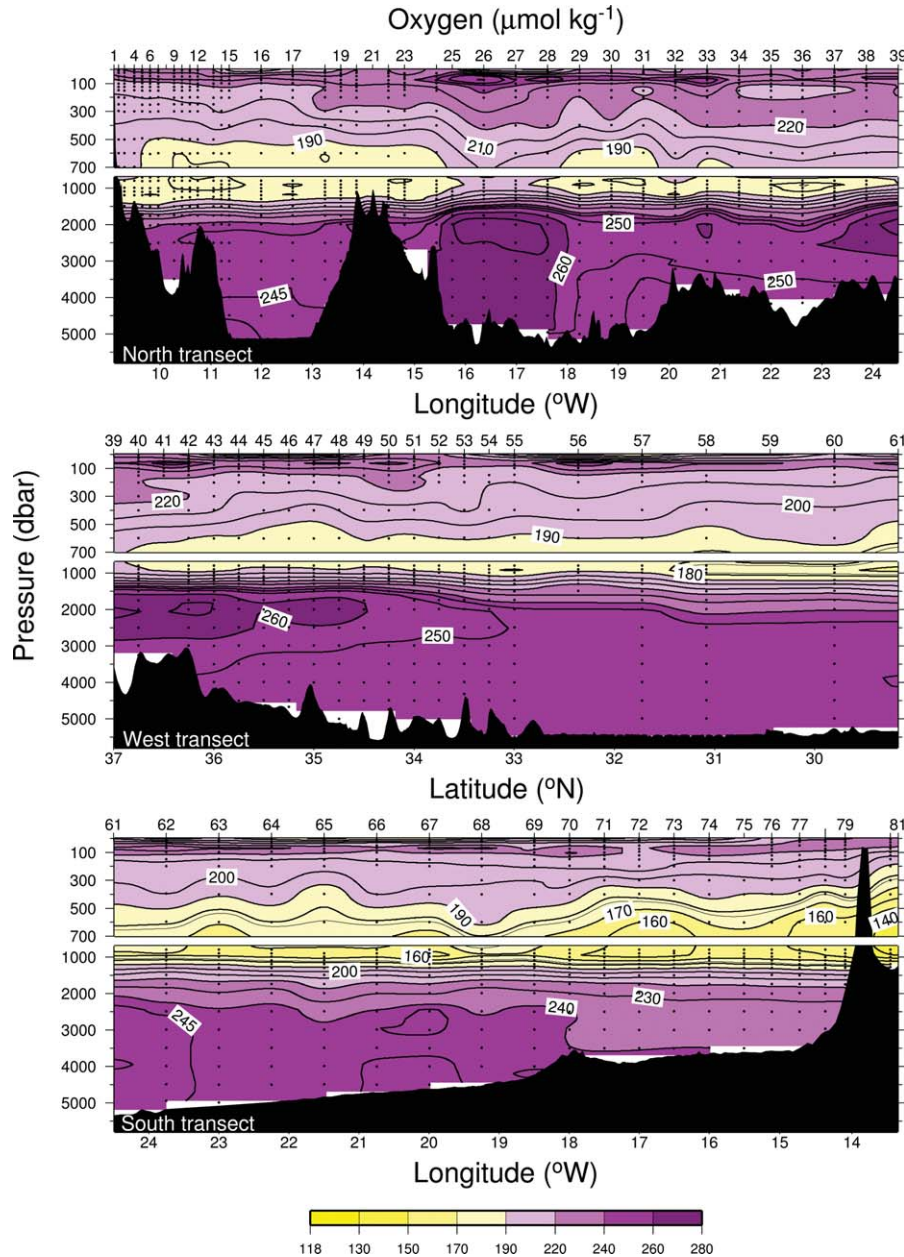


Figure 6. Vertical sections of oxygen in situ in $\mu\text{mol kg}^{-1}$ for the (top) northern, (middle) western, and (bottom) southern sections.

nutrients values corresponding to the water mass with higher/lower content of SAIW respectively. This front is marked by the isolines of 35.5 salinity (Figure 4), 180 $\mu\text{mol kg}^{-1}$ oxygen (Figure 6), 19 $\mu\text{mol kg}^{-1}$ nitrates (Figure 7), 1.25 $\mu\text{mol kg}^{-1}$ phosphates (Figure 8) and 12 $\mu\text{mol kg}^{-1}$ silicates (Figure 9). The relative high AAIW-MW and low SAIW water mass dominate the southwest corner (Figures 4 and 10, stations 58–63).

[16] Previous studies done on the Canary basin have described the intermediate waters surrounding the Canary archipelago to be a mixture of MW and AAIW [Machín *et al.*, 2010; Fraile-Nuez *et al.*, 2010]. This is observed between stations 70 and 81, where SAIW is almost negli-

ble (Figure 10). In contrast, between stations 64 and 69, more pronounced between the last two stations, the O_2/S diagram shows an increase in oxygen (Figure 10 gray asterisks). This increase is also observed in the oxygen vertical section, where the isoline 170 $\mu\text{mol kg}^{-1}$ deepens (Figure 6). In addition, stations 64–69 present a slight decrease in nutrient concentrations, shown as a deepening of the concentrations isolines 20, 1.20, and 15 $\mu\text{mol kg}^{-1}$ of nitrates (Figure 7), phosphates (Figure 8), and silicates (Figure 9), respectively. All together this indicates that between stations 64 and 69 the content of SAIW in the MW-AAIW intermediate waters mixture is higher than in the surrounding waters. Isonutrals between those stations follow

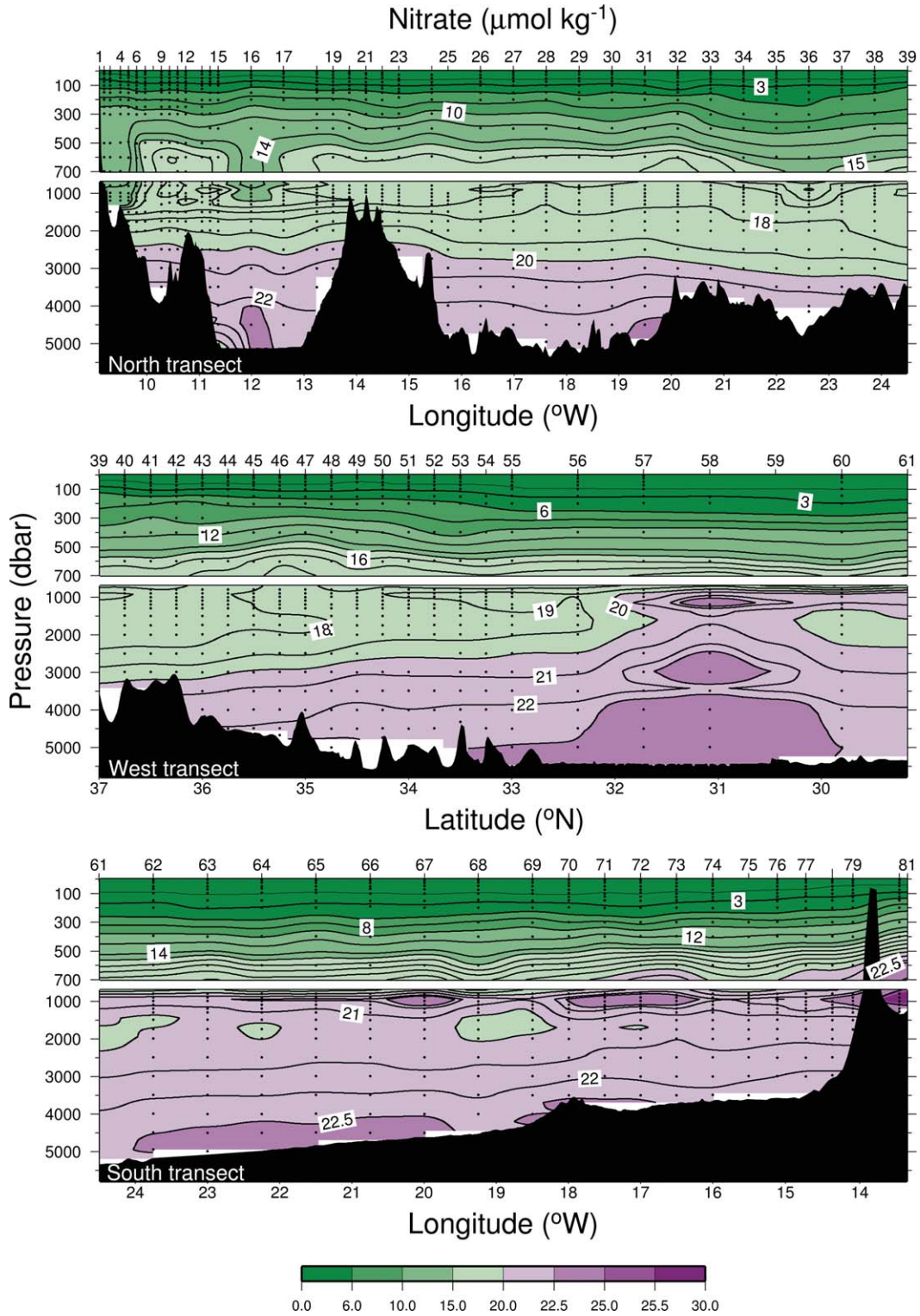


Figure 7. Vertical sections of nitrates in $\mu\text{mol kg}^{-1}$ for (top) the northern, (middle) western, and (bottom) southern sections.

the positive slope that was previously described in central waters, indicating that this water mass is flowing southward (Figure 5).

[17] Between the stations 80 and 81, hereafter Lanzarote Passage following *Hernández-Guerra et al.* [2003], inter-

mediate waters have the highest content of AAIW (Figure 10, squares). This water mass has low temperatures, salinities, and oxygen values together with high-nutrient concentrations (Figures 3, 4, and 6–9). Nitrates for diluted AAIW are about $30\ \mu\text{mol kg}^{-1}$ like in *Arhan et al.* [1994].

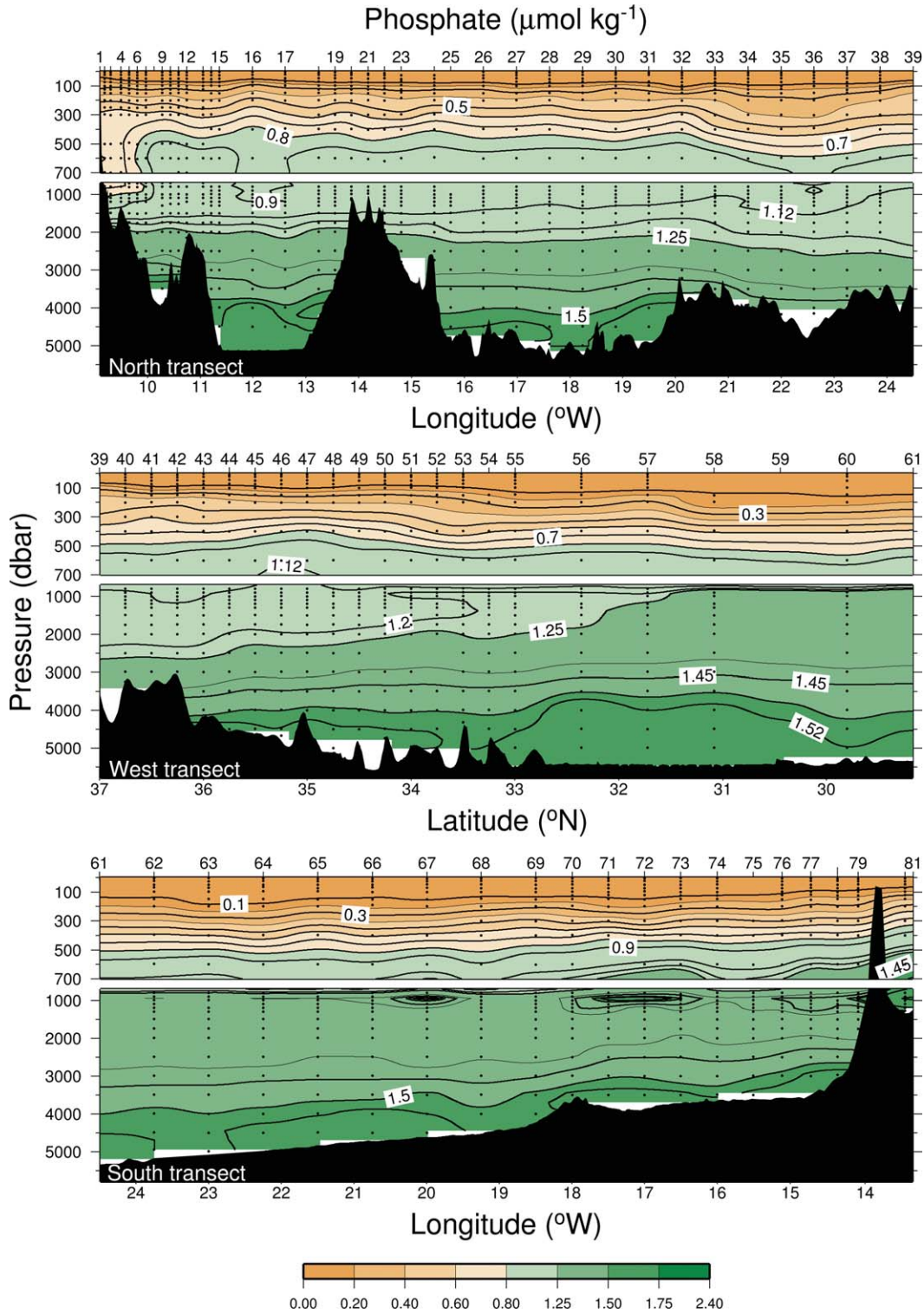


Figure 8. Vertical sections of phosphates in $\mu\text{mol kg}^{-1}$ for (top) the northern, (middle) western, and (bottom) southern sections.

The presence of this water mass in the Lanzarote Passage has been widely studied [Hernández-Guerra *et al.*, 2005; Machín *et al.*, 2006; Fraile-Nuez *et al.*, 2010].

[18] Deep and bottom water masses are found below the $\gamma_n \approx 27.9220 \text{ kg m}^{-3}$ and the $\theta \approx 6^{\circ}\text{C}$ (Figures 3 and

5). North Atlantic Deep Water (NADW), the main deep water mass of the region, occupies approximately the following ranges of temperature, salinity and oxygen, $1.95\text{--}6^{\circ}\text{C}$, $34.95\text{--}35.00$, and $230\text{--}250 \mu\text{mol kg}^{-1}$, respectively. The upper limit of NADW is marked by the isolines of

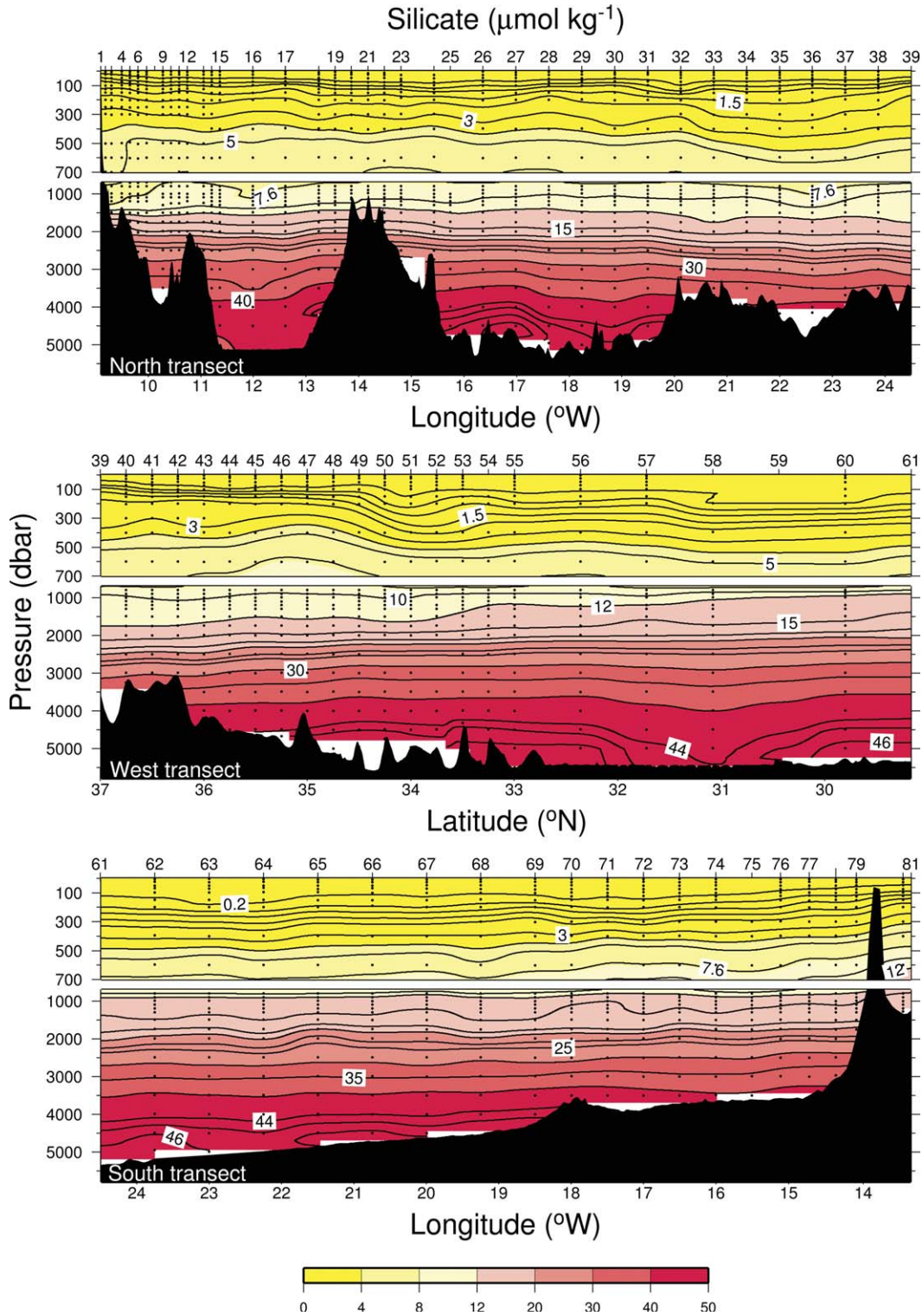


Figure 9. Vertical sections of silicates in $\mu\text{mol kg}^{-1}$ for (top) the northern, (middle) western, and (bottom) southern sections.

nitrate $\approx 19 \mu\text{mol kg}^{-1}$ and silicates $\approx 15 \mu\text{mol kg}^{-1}$ with the lower limit at temperature and salinity of 1.95°C and 34.89 . These limits have been reported by *Castro et al.* [1998] and *Kawase and Sarmiento* [1986] for the upper limit and in *Castro et al.* [1998] and *Pérez et al.* [2001] for the lower limit.

[19] Labrador sea water (LSW) is seen in Figure 2 forming a thick line over NADW with relative lower salinities and higher temperatures. Between stations 32 and 49 (northwest corner of the study area), LSW is responsible for the rise of the isotherms and isohalines observed where high-oxygen concentrations are also visible (Figures 3, 4,

Table 1. Neutral Density Levels Used in the Analysis and Approximate Equivalences With Water Masses

Layer	γ_n (kg m ⁻³) ^a	Water Mass
1	26.8500	NACW
2	27.0354	NACW
3	27.1620	NACW
4	27.3800	NACW
5	27.6200	MW/SAIW/AAIW
6	27.8200	MW/SAIW/AAIW
7	27.9220	MW/SAIW
8	27.9750	LSW/NADW
9	28.0080	LSW/NADW
10	28.0440	NADW
11	28.0720	NADW
12	28.0986	NADW
13	28.1100	NADW
14	Bottom	NADW/AABW

^aThe corresponding density value is the lower limit of each layer.

and 6). Nutrient values of LSW agree with *Van Aken* [2000a, 2000b] being 17–18, 1.12, and 10 $\mu\text{mol kg}^{-1}$ for nitrates, phosphates and silicates, respectively (Figures 7, 8, and 9). LSW produces a deepening of the 18 and 12 $\mu\text{mol kg}^{-1}$ isolines of nitrates and silicates (Figures 7 and 9).

[20] Near the bottom of the θ/S diagram, Antarctic bottom water (AABW) is observed with temperatures and salinities below $\theta \sim 2^\circ\text{C}$ and 34.85, respectively (Figure 2). AABW appears very diluted in the southwest corner of the region (Figures 3 and 4 of the west and south transects). This water mass has $>22 \mu\text{mol kg}^{-1}$ of nitrates, 1.52 $\mu\text{mol kg}^{-1}$ of phosphates and 46 $\mu\text{mol kg}^{-1}$ of silicates.

4. Initial Geostrophic Transport

[21] The neutral density level of $\gamma_n = 28.0720 \text{ kg m}^{-3}$ (ca.3000 dbar) is chosen as reference level following *Ganachaud* [2003a] for the North Atlantic Ocean and *Hernández-Guerra et al.* [2005] for the Canary Basin. Station pairs shallower than this neutral density use the bottom as reference level. The water column is divided into 14 neutral density layers (Table 1). The NACW is located in the first four layers, the intermediate water masses on the next three and the deep and bottom water masses below these. *Comas-Rodríguez et al.* [2011] have previously used these layers in the study of the Azores Current System.

[22] In Figure 11, the integrated mass, salinity anomaly and heat anomaly transports for each transect and the divergence are shown per density layer. The sign indicates positive/negative for divergence/convergence flow, out/in the box. Ekman transport is added to the first layer. As seen in the Figure 11a, the integrated mass transport shows an imbalance of -1.96 , 0.35 , and -3.83 Sv in the surface, intermediate and the deep layers, respectively. In addition, the anomaly transports (Figures 11b and 11c) have a positive/outflow net transport down to $\gamma_n = 27.9220 \text{ kg m}^{-3}$ and a negative/inflow values below it, that become zero at $\gamma_n = 28.0080 \text{ kg m}^{-3}$. In the next section an inverse box model is applied to conserve mass, salinity anomaly and heat anomaly transports.

5. Inverse Model

5.1. Model

[23] An inverse box model is applied to the box of hydrographic data shown in Figure 1. This model provides an efficient method to obtain absolute geostrophic flow using the thermal wind equation after calculating the reference level velocities and their uncertainties. These velocities are calculated assuming geostrophy and mass and properties conservation.

[24] In this study, we have extended the inverse model described in *Joyce et al.* [2001] to include the approximate conservation of mass and anomalies of salinity and heat, and to allow the transfer between layers, as in *Hernández-Guerra et al.* [2005]. This model also considers adjustment of fresh water flux and Ekman transports in each section. The mass and property equations for a closed volume are respectively:

$$\int \int \rho b dx dz + A_z \times (w^* \bar{\rho}) = - \int \int \rho v_{rel} dx dz + Q, \quad (1)$$

$$\int \int \rho (C - \bar{C}) b dx dz + A_z \times \left(w^* \bar{\rho} (C_i - C) - k_z^* \frac{\partial(\rho C)}{\partial z} \right) = - \int \int \rho (C - \bar{C}) v_{rel} dx dz + \bar{C} \times Q, \quad (2)$$

where ρ , C , \bar{C} and \bar{C}_i are the density, the property concentration per unit of mass, the mean property concentration in each layer and the mean property concentration in every interface, respectively. A_z is the horizontal area of a given neutral surface bounded by the four sections and the African and Iberian Peninsula coasts. w^* is the equivalent average dianeutral velocity across the interfaces, k_z^* is the average dianeutral diffusivity across the interfaces and Q takes into account the possible source or sink of any property such as freshwater flux or Ekman transport. The first and last integral terms of both equations comes from the reference velocities (b) and the relative velocity (v_{rel}),

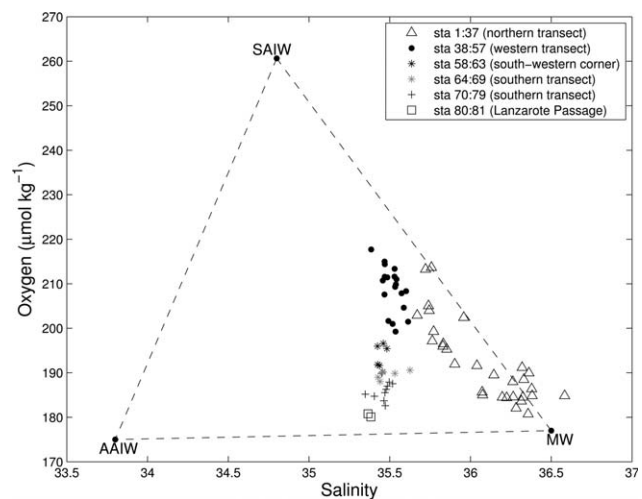


Figure 10. Oxygen ($\mu\text{mol kg}^{-1}$) versus salinity at the isopycnal surface of $\gamma_n \approx 27.8000 \text{ kg m}^{-3}$.

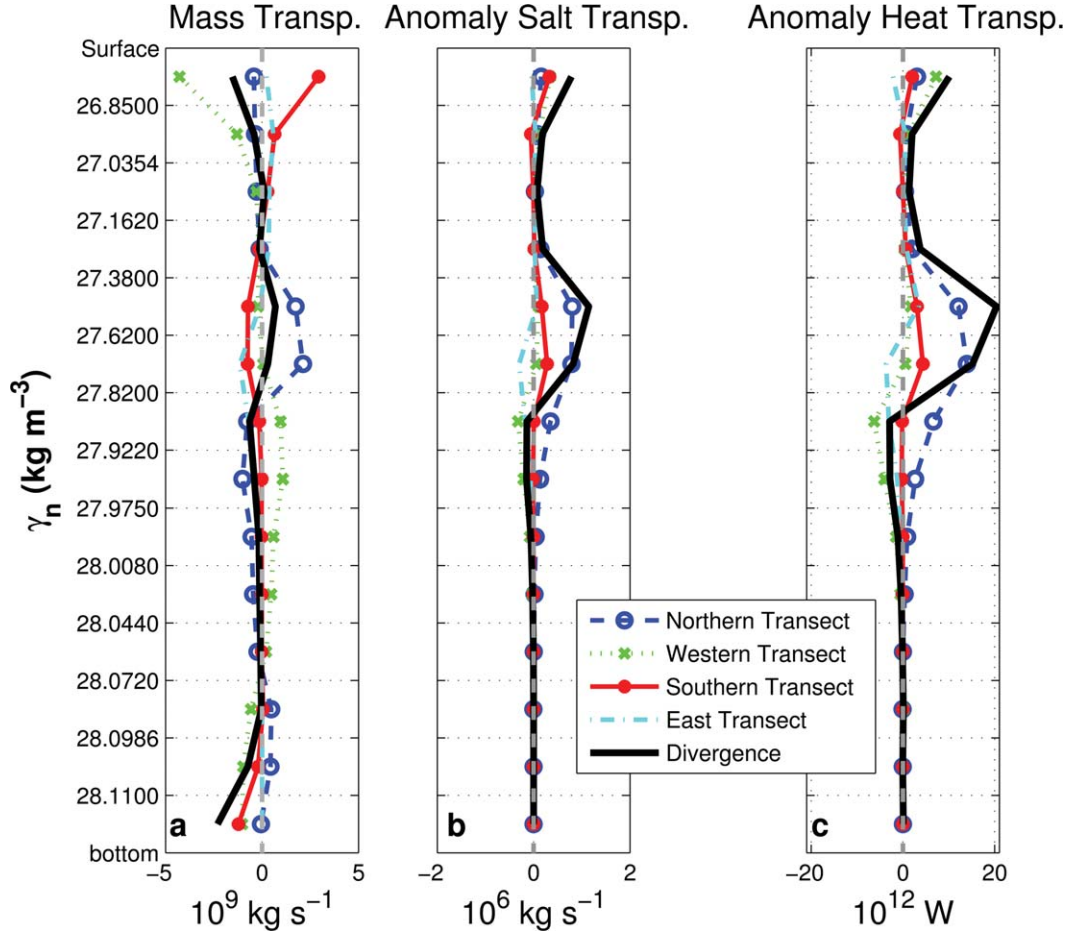


Figure 11. (a) Integrated mass, (b) salt anomaly, and (c) heat anomaly geostrophic transports. The sign indicates positive/negative for divergence/convergence flow out/in the box. Each line corresponds to the northern (circles over a dashed line), western (crosses over a dotted line), south (dots over a thin solid line), and eastern transects (dashdot line). The divergence of mass, salinity and heat anomalies are shown as a thick solid line. Different x axis scales are used.

respectively. In contrast, the second term relates to the vertical transfer for each layer.

[25] Equations of mass and salinity anomaly conservation (per layer and the total), heat anomaly conservation (from the eighth layer to the bottom to take into account atmosphere-ocean exchange) form the following matrix equation:

$$Ax + n = -\Gamma, \quad (3)$$

where A is a matrix with a size of layers (Q) \times stations (N), n is a column vector ($Q \times 1$) whose elements are the noise of each equation, Γ is a vector representing the amount by which mass or anomalies of properties are initially imbalanced in each layer ($Q \times 1$), and x is the column vector ($N \times 1$) containing the unknowns of the system:

$$\begin{pmatrix} (b_i)_i = 1, \dots, N_{pair} \\ (w_k^*)_k = 1, \dots, M_{layer} - 1 \\ (k_k^*)_k = 1, \dots, M_{layer} - 1 \\ \Delta T_{Ek} \\ \Delta F_w \end{pmatrix} \quad (4)$$

Table 2. A Priori Estimates of the Unknowns

Variables	Preliminary Variances
Shallow stations reference velocities	$(0.05 \text{ ms}^{-1})^2$
Open ocean reference velocities	$(0.02 \text{ ms}^{-1})^2$
Vertical velocity	$(10^{-6} \text{ ms}^{-2})^2$
Vertical diffusivity	$(10^{-4} \text{ ms}^{-1})^2$
Ekman transport northern transect	10% of the initial value
Ekman transport western transect	30% of the initial value
Ekman transport southern transect	10% of the initial value
Ekman transport eastern transect	50% of the initial value
Freshwater flux	50% of the initial value

[26] The inverse problem consists of 37 equations and 130 unknowns comprised of 99 for reference velocities, 26 for vertical velocities and vertical diffusion, 4 for Ekman transports and 1 for the freshwater flux. To solve the inverse problem, we have used the Gauss-Markov method which produces a minimum error variance solution from initial estimates of the unknowns. The preliminary

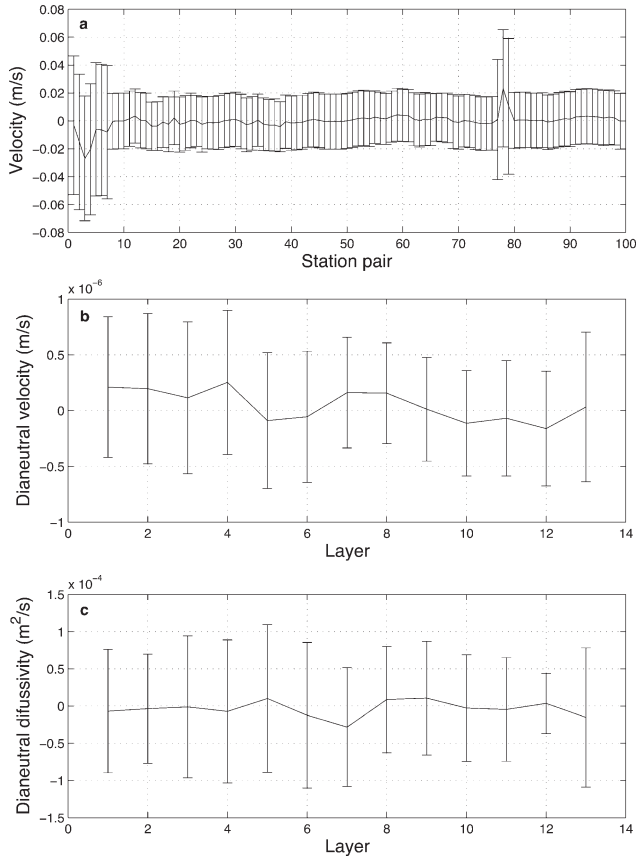


Figure 12. (a) Velocities at the reference level for each station pair, (b) dianeutral velocities, and (c) dianeutral diffusivities between layers determined by inverse calculations with their error bars.

variances assigned are shown in Table 2. The preliminary variances assigned to the unknowns of the reference velocities are higher in station pairs closer the coast than the unknowns of station pairs in the open ocean. The preliminary variance imposed for the dianeutral advection and diffusivity have been previously used in *Toole and Warren [1993]*, *Ganachaud [2003b]*, and *Hernández-Guerra et al. [2005]*. Ekman transports were estimated using winds from the NCEP and QS. Ekman transport preliminary variances come from the percentage of difference between estimations for each transect. The initial Ekman transports are -0.3 , -0.1 , 0.2 , and -0.1 Sv for the north, west, south and east transects respectively. Freshwater flux a priori variance comes from SMD94.

[27] *Ganachaud [2003b]* established that the biggest source of uncertainty in conservation equations arises from the deviation of the baroclinic mass transport, at the time of the cruise, from their mean value. Following this, the preliminary variance for each constraint was estimated in the same way as in *Hernández-Guerra et al. [2005]*, where it is established that previous studies on the region done with moored current meters and expandable bathythermographs, show that the deviation of the baroclinic mass transport from their mean value is of the same order of magnitude than the mean flow. Then, the a priori variance of mass transport imposed is $(1.5 \text{ Sv})^2$ for the thermocline layers, $(1$

$\text{Sv})^2$ for the intermediate layers, $(0.5 \text{ Sv})^2$ for the deep layers and $(4 \text{ Sv})^2$ for the total.

5.2. Results

[28] As result of the inverse model, Figure 12a shows the velocities at the reference layer together with their error bars obtained from the inverse model. The velocities are small, most of them being in the range $\pm 1 \text{ cm s}^{-1}$, except in between stations 2 and 3, 3 and 4, 4 and 5, and 78 and 79 whose values vary between $\pm 3 \text{ cm s}^{-1}$. These values correspond to San Vicente Cape and to the Lanzarote Passage, both shallow areas where the flow is stronger [*Laiz et al., 2012*]. The uncertainties are quite similar to the a priori variances imposed which agree with other inverse model results [*Ganachaud et al., 2000*].

[29] In Figures 12b and 12c, the vertical velocities and the dianeutral diffusivities present small values not significantly different from zero. The Ekman transports adjusted to the inverse model become, -0.3 ± 0.03 Sv, 0.1 ± 0.03 Sv, -0.2 ± 0.02 Sv and -0.1 ± 0.05 Sv for the north, west, south and east sections, respectively. Freshwater flux was originally -2.7×10^{-2} Sv and with the adjustment becomes $(-1.5 \pm 1.2) \times 10^{-2}$ Sv, that is not significantly different of the provided by the climatology but different from zero. This result indicates that evaporation is taking place as in *Dobroliubov [1998]*. Atmosphere-ocean heat exchange is also obtained from the inverse model, being $(-14.3 \pm 50.2) \times 10^{-3}$ PW (1 PW = 10^{15} W). Considering the whole surface oceanic area bounded by the stations, the corresponding heat is $-11.26 \pm 39.5 \text{ W m}^{-2}$, not significantly different than zero.

[30] Figure 13 shows that the uncertainty for the mass transport in each layer is greater than the imbalance (Figure 13a). The net mass imbalance is -0.7 ± 2.2 Sv. Then, in each layer and the total imbalance are not significantly different from zero. Anomaly salt transport divergence is always less than $-0.8 \times 10^6 \text{ kg s}^{-1}$ and is indistinguishable from zero in all layers except the first layer which is $(1.1 \pm 0.5) \times 10^6 \text{ kg s}^{-1}$ and the fifth layer which is $(0.6 \pm 0.3) \times 10^6 \text{ kg s}^{-1}$. The comparison between Figure 11 and Figure 13 shows an improvement in the mass and properties conservation for each layer.

6. Adjusted Geostrophic Transport

[31] In order to better understand the results, hereafter geographical sign will be used in the text (positive north and east, negative south and west). In the north transect (Figure 14a), northward flow of thermocline (2.0 ± 0.4 Sv) and intermediate (2.7 ± 0.9 Sv) waters are found from 9.6°W to 11.4°W (stations 5–15). Figure 4 shows that the intermediate northward flow is mainly MW. *Mauritzen et al.'s [2001]* ADCP charts show a similar northward transport. They used a section at $8^\circ 20'\text{W}$ to estimate the northward flow through the Gulf of Cadiz and they found 4.2 ± 1.1 Sv in intermediate waters and 1.6 ± 0.7 Sv in the thermocline layers. This northward flow is also observable in *Peliz et al. [2005]* where it is considered a warm inflow from the Gulf of Cadiz generated by a northward recirculation of the Azores Current.

[32] Further west, surface waters flow southward carrying -1.8 ± 0.4 Sv between 13.5°W and 14.8°W (stations

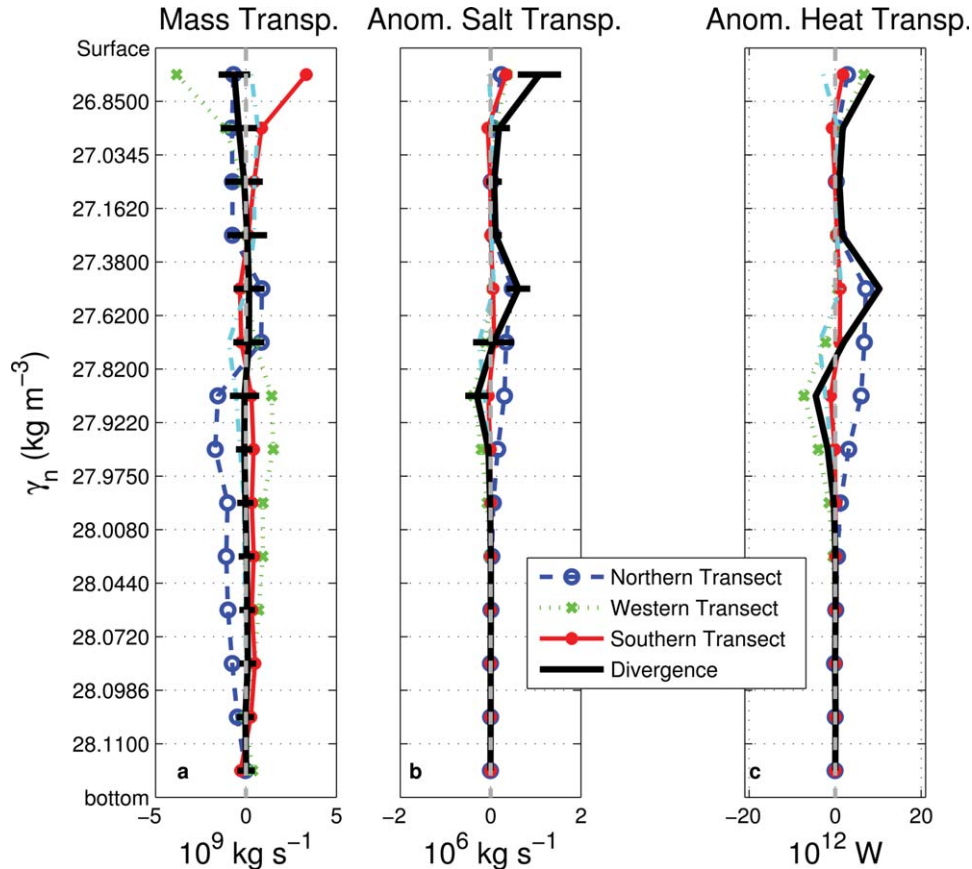


Figure 13. (a) Integrated mass, (b) salt anomaly, and (c) heat anomaly transports using the results of the inverse model together with their error. The sign indicates positive/negative for divergence/convergence flow out/in the box. Each line corresponds to the northern (circles over a dashed line), western (crosses over a dotted line), south (dots over a thin solid line), and eastern transects (dashdot line). The divergence of mass, salinity and heat anomalies are shown as a thick solid line. Different x axis scales are used.

19–23). At the intermediate layers a nonsignificant transport of -0.6 ± 0.6 Sv is observed. The oxygen vertical section shows that the surface southward flow transports waters with a higher oxygen concentration, indicating that it is the weak Portugal Current (Figure 6).

[33] In the northern transect, three anticyclonic eddies can be observed between stations 15 and 19, 23 and 25, and 32 and 41 (Figures 4 and 5). The last eddy is the largest one extending to the beginning of the western transect. *Comas-Rodríguez et al.* [2011] also show this anticyclonic eddy with altimetry data in their Figure 8a. Oceanic islands are an obstacle for currents which are forced to flow around them, generating cyclonic/anticyclonic eddies to the right/left side, downstream of the islands. This phenomenon has been widely documented in the case of the Canary Islands [*Hernández-Guerra et al.*, 1993; *Pacheco and Hernandez-Guerra*, 1999], and in the Azores Archipelago [*Pérez et al.*, 2003; *Siedler et al.*, 2005]. In this case, the position of the anticyclonic eddy discards this hypothesis. It has also been described the existence of anticyclonic/cyclonic eddies in the northern/southern flanks of the Azores Current [*Alves and Colin de Verdière*, 1999; *Barbosa et al.*, 2011]. From a year of altimeter data, it is observed that the eddy between the stations 32 and 41 originates from a meander of the Azores Current as shown in the simplified model of *Alves*

and *Colin de Verdière* [1999], and that the eddy propagates westward through the north Azores Current corridor described in *Sangrà et al.* [2009].

[34] The Azores Current System is seen in the western transect (Figure 14b). The Azores Countercurrent ($35.25\text{--}36.25^\circ\text{N}$, stations 42–46) transports westward -3.4 ± 0.3 Sv in the thermocline layers and -2.6 ± 0.5 Sv in the intermediate layers. In the latitude range $33.5\text{--}34.5^\circ\text{N}$ (stations 49–53), the Azores Current carries eastward 10.6 ± 0.4 Sv in the thermocline layers and 3.7 ± 0.6 Sv in the intermediate layers. This means that the Azores Current System is transporting eastward 7.2 ± 0.5 Sv in the surface layers and 1.1 ± 0.8 Sv at intermediate layers. These values are the same, with their error estimates, as the ones reported by *Comas-Rodríguez et al.* [2011].

[35] Three eddies, two cyclonic (at stations 53–58 and 61–64) and one anticyclonic (between stations 58 and 61) separate the Azores Current System from the Canary Current. The Canary Current extends from 22.25°W to 18.50°W (stations 64–69) in the south transect, west of La Palma island, the north-westernmost island of the Canaries. The Canary Current presents a southward thermocline mass transport of -6.2 ± 0.6 Sv (Figure 14c). It is worth

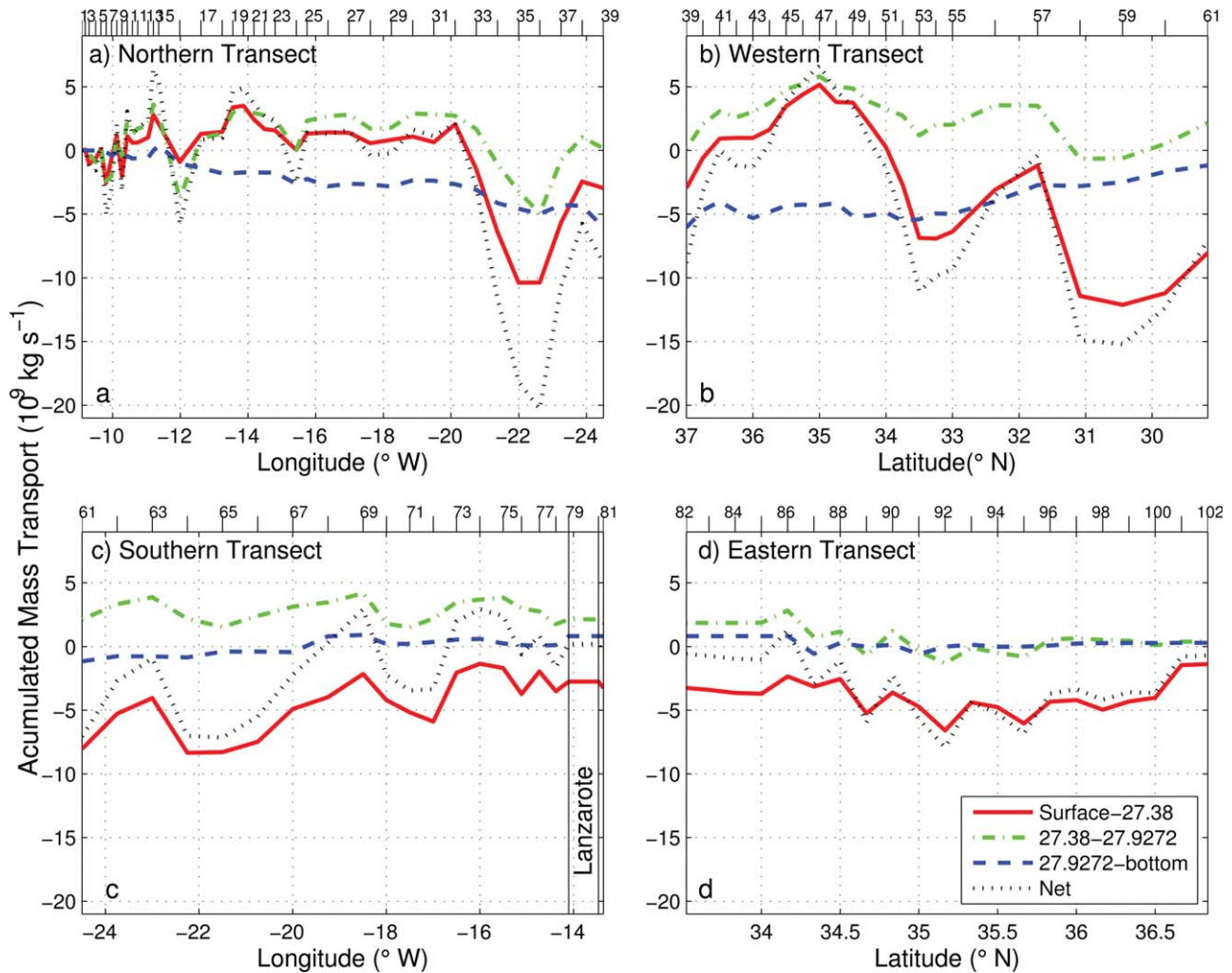


Figure 14. Accumulated mass transport in Sv for the (a) northern, (b) western, (c) southern, and (d) eastern transects. The x axis for the northern and southern transects is longitude ($^{\circ}$ W) while for the western and eastern transects is latitude ($^{\circ}$ N). The station number is located on the top axis of each subplot. Thermocline layers (1–4) are shown with red lines, intermediate layers (5–7) with dash-dot green lines, deep layers (8–14) with dashed blue lines and the net transport with dashed black lines.

mentioning that a southward flow of -2.0 ± 0.8 Sv is recorded in intermediate waters immediately below the Canary Current. This intermediate flow has a mixture MW-AAIW from the region plus a contribution of SAIW as seen in Figure 10.

[36] In the Lanzarote Passage, a northward flux of 0.5 ± 0.1 Sv and 0.3 ± 0.1 Sv in the thermocline and intermediate layers is found (Figure 15). The northward transport of NACW in the Lanzarote Passage in fall is in agreement with the 1.1 ± 0.5 Sv obtained in *Hernández-Guerra et al.* [2005] with an inverse model and with the fall values of 1997 (0.48 ± 0.59 Sv), 2000 (0.51 ± 0.42 Sv), and 2001 (0.86 ± 2.52 Sv) estimated from mooring data in *Fraile-Nuez et al.* [2010]. The transport at intermediate levels has the higher content of AAIW. The obtained 0.3 ± 0.1 Sv of AAIW is in agreement with the 0.1 ± 0.4 Sv and 0.7 ± 0.5 Sv estimated in *Hernández-Guerra et al.* [2003] and *Hernández-Guerra et al.* [2005], respectively, and also with the 9 year mean of 0.09 ± 0.57 Sv obtained in *Fraile-Nuez et al.* [2010]. In *Laiz et al.* [2012], the Lanzarote Passage is studied with different

expendable bathythermograph (XBT) and CTD tracks obtaining a mean northward transport of 1.8 ± 0.7 Sv in fall and early winter, which is slightly higher to our 0.8 ± 0.1 Sv.

[37] The adjacent Mediterranean Sea exchanges 1.9 ± 0.5 Sv (eastward/inflow) and -1.5 ± 0.8 Sv (westward/outflow) of surface and intermediate water masses, respectively, with the Atlantic Ocean (Figure 14d). These transports are not significantly different that those reported by *Baringer and Price* [1997], who obtained an outflow of 1.88 Sv and an inflow of 1.79 Sv from CTD and XBT data.

[38] The deep water masses enter the region carrying -5.0 ± 3.1 Sv across the north transect, between 9.6 and 22.6° W (stations 5–36) and leave the area (-4.1 ± 2.8 Sv) at the southwestern corner of the box from 33.0° N– 24.5° W to 29.2° N– 22.3° W (between stations 55 and 64). This deep circulation scheme is similar to the one shown in *Paillet and Mercier* [1997] (their Figure 7e). Since *Defant* [1941] a southward flow of NADW in the Atlantic eastern basin has been reported [*Maillard*, 1986; *Gana and Provost*, 1993]. AABW can be found only in the southwestern

ORCA 1009

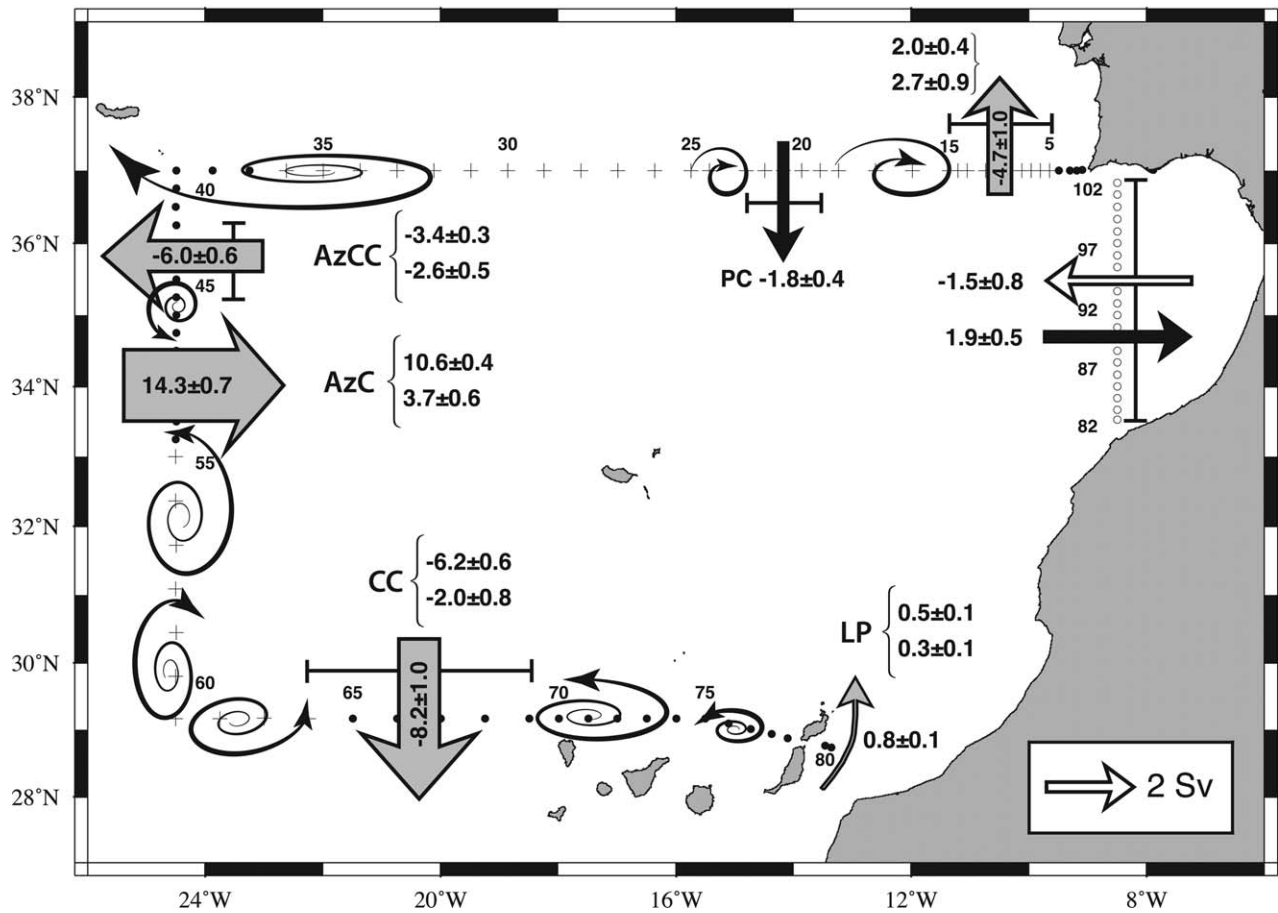


Figure 15. Main currents with their corresponding integrated mass transport (in Sv). PC, AzCC, AzC, CC, and LP stand for Portugal Current, Azores Countercurrent, Azores Current, Canary Current, and Lanzarote Passage, respectively. Curly brackets indicate (top) the surface and (bottom) intermediate mass transport for each current. Gray arrows and the enclosed number, correspond to the integrated surface and intermediate transport. The exchange between the Mediterranean Sea and the Atlantic Ocean is shown with black arrows (surface layers) and white arrows (intermediate layers). The width of the arrow shaft is proportional to the mass transport values. Spiral arrows indicate the presence of an anticyclonic/cyclonic eddy. The stations where deep circulation was found are shown with black crosses instead of black dots (ORCA stations) or white dots (WOCE AR06 stations).

corner of the geographical area between the stations 57 and 61, but it presents a transport non significantly different than zero. The position found for this water mass is quite similar to the one reported in *Hernández-Guerra et al.* [2005].

7. Discussion and Conclusions

[39] An inverse box model has been applied to the geographical region of 28.7–37.0°N, 9.1–24.5°W in order to estimate the circulation in the northeast subtropical gyre of the Atlantic Ocean and to infer the source of the Canary Current in fall of 2009.

[40] The Portugal current is found between 13.5°W and 14.8°W (stations 19–23) carrying -1.8 ± 0.4 Sv (Figure 15). This position and transport is in agreement with that from *Stramma* [1984], *Schmitz* [1996], and *Paillet and Mercier* [1997]. In previous works, it is observed that the

southward Portugal Current merges with the Azores Current and forms the Mediterranean inflow [*Stramma*, 1984; *Stramma and Isemer*, 1988; *Stramma and Müller*, 1989; *Stramma and Siedler*, 1988; *Schmitz*, 1996; *Paillet and Mercier*, 1997].

[41] The Azores Current System is located south of a wide anticyclonic eddy. The Azores Countercurrent transports westward -3.4 ± 0.3 Sv in the thermocline layers and -2.6 ± 0.5 in the intermediate layers (mainly MW) between 35.25–36.25°N (Figure 15). The Azores Current (33.50–34.50°N) transports 10.6 ± 0.4 Sv eastward at thermocline layers and 3.7 ± 0.6 Sv at intermediate layers (mainly SAIW). These values are in agreement with those from *Comas-Rodríguez et al.* [2011] using lowered acoustic Doppler current profiler data and to the previously estimated for the Azores Current [*Paillet and Mercier*, 1997; *Jia*, 2000]. Between both currents an eddy is observed. The presence of the Azores Front (approximately at 33.75°N) in

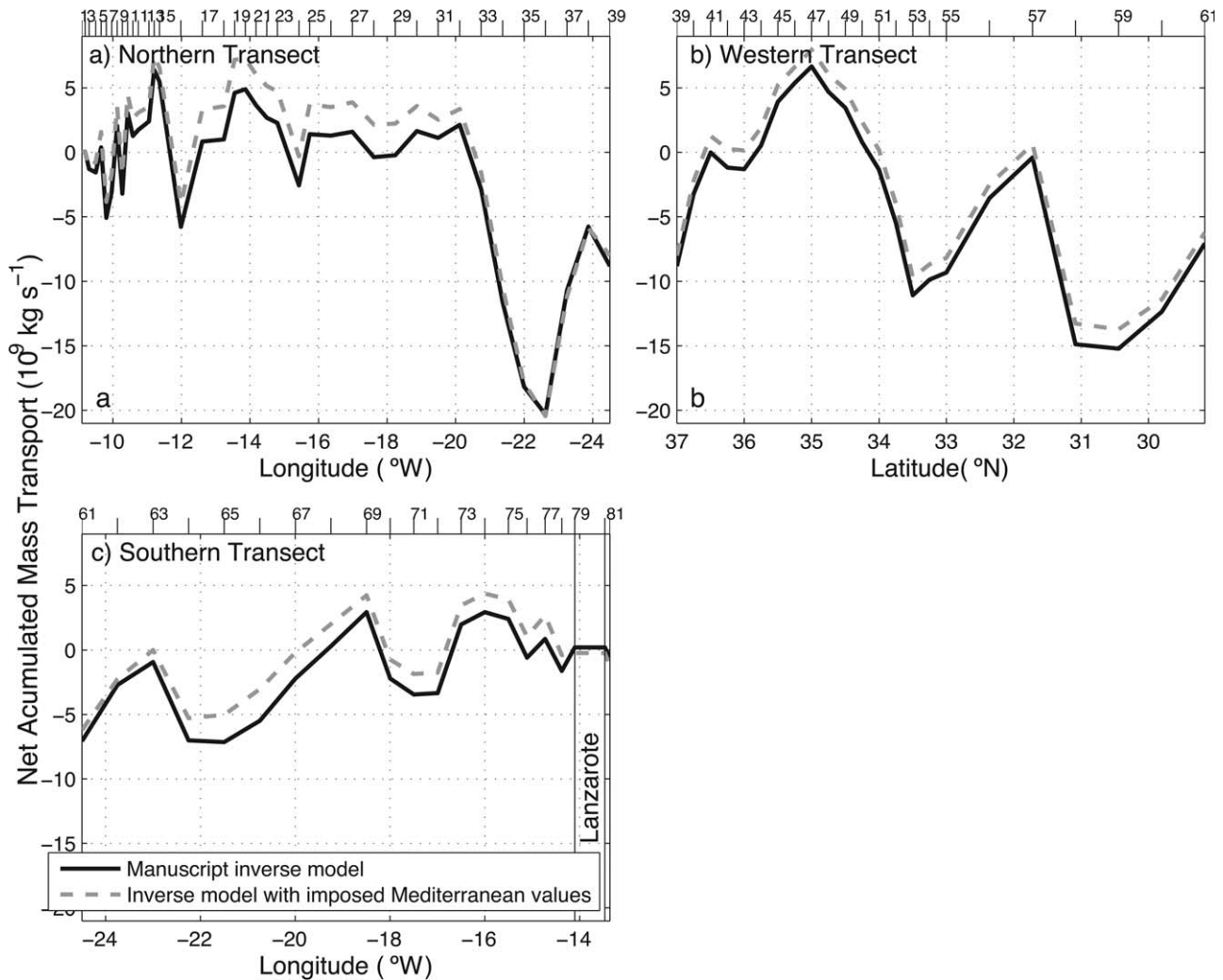


Figure A1. Net transport per transect of the inverse model of the manuscript (black line) and the inverse model done with imposed values for the Mediterranean inflow/outflow (gray line). (a) Northern transect, (b) Western transect, and (c) Southern transect.

the middle-south part of the Azores Current, divides the cool waters (north) from the warm waters (south) in the first 700 dbar. The presence of this front associated with the Azores Current has been described previously in *Alves and Colin de Verdière* [1999], *Pérez et al.* [2003], *Siedler et al.* [2005], and *Kida et al.* [2008]. The maximum eastward flow of the Azores Current is associated with the Azores Front as in *Comas-Rodríguez et al.* [2011].

[42] Our results show a Canary Current flowing in the westernmost position ever observed. The surface mass transport is in agreement with the 5.8 ± 0.6 Sv found in *Hernández-Guerra et al.* [2005] and with the 6 Sv of *Paillet and Mercier* [1997]. This transport in the thermohaline layer is slightly higher than the reported in *Machín et al.* [2006] and in *Fraile-Nuez and Hernández-Guerra* [2006]. In *Machín et al.* [2006], the fall season is described as a period where the flow intensifies and moves offshore. In fall 2009, the Canary Current has shifted further west and transports higher mass to the south. From 1 April 2009 to 31 March 2010, *McCarthy et al.* [2012] found that the Meridional Overturning Circulation strength dropped below its

mean value. They attribute it to an intensification of the southward upper mid-ocean transport caused by a deepening of the thermocline on the western boundary and an anomalously negative Ekman transport. These conditions found in fall 2009 could explain the western shift and strengthening of the Canary Current.

[43] The model results and all the above discussion, suggest the following circulation in the thermocline (Figure 15). Most of the Azores Current feeds the Canary Current in the surface layers. A slide of the Azores Current flows eastward and suffers the rectification of the mesoscale turbulent eddies that generates a westward surface flow north of it [*Alves and Colin de Verdière*, 1999]. This westward surface flow is the surface Azores Countercurrent that carries -3.4 ± 0.3 Sv. As various studies indicate, a weak fraction of the Azores Current (1.0 ± 0.8 Sv) continues eastward and reaches the Strait of Gibraltar [*Mauritzen et al.*, 2001; *Peliz et al.*, 2005, 2007; *Kida et al.*, 2008; *Mason et al.*, 2011; *Laiz et al.*, 2012]. Between 13.5° W and 14.8° W, the southward Portugal Current merges with the weak eastward flow, augmenting the transport to

2.8 ± 0.9 Sv. This transport is very similar to the eastward contribution observed in the vicinity of the Gulf of Cadiz in Peliz *et al.* [2007] (3.2 Sv) and in Laiz *et al.* [2012] (observations 2.5 ± 0.6 Sv and model 3.9 Sv). When this merged flow reaches the Strait of Gibraltar part of it will enter in the Mediterranean Sea [Stramma and Siedler, 1988; Schmitz, 1996; Paillet and Mercier, 1997] and part will recirculate northward through the Gulf of Cadiz to Cape San Vicente [Mauritzen *et al.*, 2001; Peliz *et al.*, 2005, 2007; Kida *et al.*, 2008; Mason *et al.*, 2011; Laiz *et al.*, 2012].

[44] The circulation scheme at intermediate layers is harder to infer from Figure 15. The intermediate waters of the Azores Current are mainly composed of SAIW, and those of the Canary Current present a contribution of SAIW. Both currents present a similar mass transport. Altogether this indicates that most of the Azores Current feeds the Canary Current at intermediate layers, although, part of it continues to flow eastward (1.7 ± 1.0 Sv). Following Comas-Rodríguez *et al.* [2011], the characteristics of our Azores Current System better agrees with the β -plume formation hypothesis. Thus, the Mediterranean outflow on its way to the Atlantic Ocean generates an eastward flow that forms the Azores Countercurrent intermediate transport. This eastward flow augments its transport by entrainment and with the recirculation of the weak eastward Azores Current intermediate mass transport [Kida *et al.*, 2008; Volkov and Fu, 2010]. The Mediterranean outflow spreads and flows northward in the vicinity of Cape San Vicente [Mauritzen *et al.*, 2001; Peliz *et al.*, 2005, 2007].

Appendix A: Sensitive Analysis

[45] An inverse model requires a closed box model in order to conserve mass. ORCA cruise did not survey the exchange in the Strait of Gibraltar. In order to close the box, a Meridional section from a previous cruise is used. Another way to close the box, as done in Hernández-Guerra *et al.* [2010], is to impose mass transport values for the Strait of Gibraltar. The imposed values that are used in this sensitive analysis are taken from Hernández-Guerra *et al.* [2010]. In their work, they allow an outflow of 1 Sv into the Mediterranean as described in Candela [2001] and an entrainment of a similar volume drawn from layers 4:5 into the MW as shown by Baringer and Price [1997], which then augments the transport of layers 6:7.

[46] Here a comparison between both estimates is shown. Figure A1 shows the net accumulated mass transport estimated with both inverse models. The figure shows that both models show similar results. Furthermore, looking carefully to each main current described in the manuscript, we verified that there is not a significant difference between both estimates (considering their uncertainties).

[47] **Acknowledgments.** This work has been performed under the framework of the ORCA project (CTM2005-04701-C02-01) with contribution of the Malaspina project (CSD2008-00077), financed by the Spanish Government and Feder. The first author will like to thank the Agencia Canaria de Investigación, Innovación y Sociedad de la Información (ACIISI) grant program of Apoyo al Personal Investigador en Formación. We will also like to acknowledge the Unidad Tecnológica Marina (UTM) and BIO Hespérides captain and its crew for their collaboration and help

during the cruise. Special thanks to Johan Sebastián Cortés Montenegro and David Sosa Trejo for helping with the figures and data treatment.

References

- Alves, M. (1996), Instability dynamics of a subtropical jet: The Azores front-current system case (FCA), PhD thesis, Univ. de Bretagne Occidentale, Brest, France.
- Alves, M., and A. Colin de Verdière (1999), Instability dynamics of a subtropical jet and applications to the Azores front current system: Eddy-driven mean flow, *J. Phys. Oceanogr.*, 29(5), 837–864.
- Alves, M., F. Gaillard, M. Sparrow, M. Knoll, and S. Giraud (2002), Circulation patterns and transport of the Azores front-current system, *Deep Sea Res. Part II: Top. Stud. Oceanogr.*, 49(19), 3983–4002.
- Arhan, M., A. Colin de Verdière, and L. Mémerly (1994), The Eastern boundary of the subtropical North Atlantic, *J. Phys. Oceanogr.*, 24, 1295–1316.
- Barbosa A. A., A. Peliz, A. Pires, and B. Le Cann (2011), Zonal structure of the mean flow and eddies in the Azores current system, *J. Geophys. Res.*, 116, C02012, doi:10.1029/2010JC006538.
- Baringer, M., and J. Price (1997), Mixing and spreading of the Mediterranean outflow, *J. Phys. Oceanogr.*, 27(8), 1654–1677.
- Cabeçadas, G., M. Brogueira, and C. Goncalves (2003), Intermediate water masses off south-southwest Portugal: Chemical tracers, *J. Mar. Res.*, 61(4), 539–552.
- Candela, J. (2001), Mediterranean water and global circulation, *Int. Geophys.*, 77, 419–429.
- Carpenter, J. (1965a), The Chesapeake Bay Institute technique for the Winkler dissolved oxygen method, *Limnol. Oceanogr.*, 10(1), 141–143.
- Carpenter, J. (1965b), The accuracy of the Winkler method for dissolved oxygen analysis, *Limnol. Oceanogr.*, 10(1), 135–140.
- Carritt, D., and J. Carpenter (1966), Comparison and evaluation of currently employed modifications of the Winkler method for determining dissolved oxygen in seawater; a NASCO report, *J. Mar. Res.*, 24(3), 286–318.
- Castro, C., F. Pérez, S. Holley, and A. Ríos (1998), Characterization and modeling of water masses in the Northeast Atlantic, *Prog. Oceanogr.*, 41(3), 149–179.
- Comas-Rodríguez, I., A. Hernández-Guerra, E. Fraile-Nuez, A. Martínez-Marrero, V. Venítez-Barrios, M. Pérez-Hernández, and P. Velez-Belchí (2011), The Azores current system from a meridional section at 24.5°W, *J. Geophys. Res.*, 116, C09021, doi:10.1029/2011JC007129.
- Defant, A. (1941), Quantitative untersuchungen zur statik und dynamik des atlantischen ozeans, die absolute topographie des physikalischen meeres-niveaus und der druckflächen sowie die wasserbewegungen im raum des atlantischen ozeans, in *Wiss. Ergeb. der Deutschen Atl. Exped. auf dem Forsch. und Vermessungsschiff Meteor, 6:2nd part*, Walter de Gruyter, Berlin, Germany, pp. 191–260.
- Dobroliubov, S. (1998), Freshwater transport in the North Atlantic Ocean: Intercomparison of balance and direct estimates, *Phys. Chem. Earth*, 23(5–6), 555–560.
- Emery, W. (2003), Water types and water masses, *Encycl. Ocean Sci.*, 6, 3179–3187.
- Fiekas, V., J. Elken, T. Müller, A. Aitsam, and W. Zenk (1992), A view of the Canary Basin thermocline circulation in winter, *J. Geophys. Res.*, 97(C8), 12,495–12,510.
- Flokard, A. R. (1978), Automatic analysis of sea water nutrients, *Fish. Res. Tech. Rep.* 46, pp. 23, MAFF Direct Fish. Res., Lowestoft.
- Fraile-Nuez, E., and A. Hernández-Guerra (2006), Wind-driven circulation for the eastern North Atlantic subtropical gyre from argo data, *Geophys. Res. Lett.*, 33, L03601, doi:10.1029/2005GL025122.
- Fraile-Nuez, E., F. Machín, P. Velez-Belchí, F. López-Laatzén, R. Borges, V. Benítez-Barrios, and A. Hernández-Guerra (2010), Nine years of mass transport data in the eastern boundary of the North Atlantic subtropical gyre, *J. Geophys. Res.*, 115, C09009, doi:10.1029/2010JC006161.
- Gana, S., and C. Provost (1993), Circulation and fluxes of the central north atlantic in 1983/84 estimated by inverse analysis of topogulf hydrographic data, *J. Mar. Syst.*, 4(1), 67–92.
- Ganachaud, A. (2003a), Large-scale mass transports, water mass formation and diffusivities estimated from World ocean circulation experiment (WOCE), *J. Geophys. Res.*, 108(C7), 3213, doi:10.1029/2002JC01565.
- Ganachaud, A. (2003b), Error budget of inverse box model: The north Atlantic, *J. Atmos. Oceanic Technol.*, 20, 1641–1655.

- Ganachaud, A., C. Wunsch, J. Marotzke, and J. Toole (2000), Meridional overturning and large-scale circulation of the Indian Ocean, *J. Geophys. Res.*, 105(C11), 26,117–26,134.
- Gould, W. (1985), Physical oceanography of the Azores Front, *Prog. Oceanogr.*, 14, 167–190.
- Harvey, J. (1982), θ – S relationships and water masses in the eastern North Atlantic, *Deep Sea Res.*, 29, 1021–1033.
- Harvey, J., and M. Arhan (1988), The water masses of the central North Atlantic in 1983–1984, *J. Phys. Oceanogr.*, 18, 1855–1875.
- Hernández-Guerra, A., J. Aristegui, M. Cantón, and L. Nykjaer (1993), Phytoplankton pigment patterns in the Canary Islands area as determined using Coastal zone color scanner data, *Int. J. Remote Sens.*, 14(7), 1431–1437.
- Hernández-Guerra, A., et al. (2002), Temporal variability of mass transport in the Canary Current, *Deep Sea Res. Part II: Top. Stud. Oceanogr.*, 49(17), 3415–3426.
- Hernández-Guerra, A., et al. (2003), Transport variability in the Lanzarote passage (eastern boundary current of the North Atlantic subtropical Gyre), *Deep Sea Res. Part I*, 50(2), 189–200.
- Hernández-Guerra, A., E. Fraile-Nuez, F. Lopez-Laatzén, A. Martínez, G. Parrilla, and P. Velez-Belchí (2005), Canary current and north equatorial current from an inverse model, *J. Geophys. Res.*, 110, C12019, doi:10.1029/2005JC003032.
- Hernández-Guerra, A., T. Joyce, E. Fraile-Nuez, and P. Vélez-Belchí (2010), Using Argo data to investigate the meridional overturning circulation in the North Atlantic, *Deep Sea Res. Part I*, 57(1), 29–36, doi:10.1016/j.dsr.2009.10.003.
- Jia, Y. (2000), Formation of an Azores Current due to Mediterranean overflow in a modeling study of the North Atlantic, *J. Phys. Oceanogr.*, 30, 2345–2358.
- Joyce, T., A. Hernández-Guerra, and W. Smethie (2001), Zonal circulation in the NW Atlantic and Caribbean from a meridional WOCE hydrographic section at 66°W, *J. Geophys. Res.*, 106, 22,095–22,113.
- Käse, R., and G. Siedler (1982), Meandering of the subtropical front south-east of the Azores, *Nature*, 300, 245–246, doi:10.1038/300245a0.
- Kawase, M., and J. Sarmiento (1986), Circulation and nutrients in middepth Atlantic waters, *J. Geophys. Res.*, 91(C8), 9749–9770.
- Kida, S., J. Price, and J. Yang (2008), The upper-oceanic response to overflows: A mechanism for the Azores Current, *J. Phys. Oceanogr.*, 38, 880–895.
- Klein, B., and G. Siedler (1989), On the origin of the Azores Current, *J. Geophys. Res.*, 94(C5), 6159–6168.
- Krauss, W., and C. Wuebbler (1982), Response of the North Atlantic to annual wind variations along the eastern coast, *Deep Sea Res. Part I*, 29(7), 851–868.
- Laiz, I., J. Pelegrí, F. Machín, P. Sangrà, A. Hernández-Guerra, A. Marrero-Díaz, and A. Rodríguez-Santana (2012), Eastern boundary drainage of the North Atlantic subtropical gyre, *Ocean Dyn.*, 62(9), 1287–1310, doi:10.1007/s10236-012-0560-6.
- Machín, F., A. Hernández-Guerra, and J. Pelegrí (2006), Mass fluxes in the Canary Basin, *Prog. Oceanogr.*, 70(2–4), 416–447.
- Machín, F., J. L. Pelegrí, P. Velez-Belchí, F. López-Laatzén, and A. Hernández-Guerra (2010), Seasonal flow reversals of intermediate waters in the Canary Current system east of the Canary Islands, *J. Phys. Oceanogr.*, 40, 1902–1909.
- Maillard, C. (1986), Atlas hydrologique de l'atlantique nord-est, in *IFREMER, IFREMER - Institut Français de Recherche pour l'Exploitation de la Mer*, France, pp. 133.
- Mason, E., F. Colas, J. Molemaker, A. Shchepetkin, C. Troupin, J. McWilliams, and P. Sangrà (2011), Seasonal variability of the Canary Current: A numerical study, *J. Geophys. Res.*, 116, C06001, doi:10.1029/2010JC006665.
- Mauritzen, C., Y. Morel, and J. Paillet (2001), On the influence of Mediterranean water on the central waters of the North Atlantic Ocean, *Deep Sea Res. Part I*, 48(2), 347–381.
- McCarthy, G., E. Frajka-Williams, W. Johns, M. Baringer, C. Meinen, H. Bryden, D. Rayner, A. Duchez, C. Roberts, and S. Cunningham (2012), Observed interannual variability of the atlantic meridional overturning circulation at 26.5°N, *Geophys. Res. Lett.*, 39, L19609, doi:10.1029/2012GL52933.
- Onken, R. (1993), The Azores countercurrent, *J. Phys. Oceanogr.*, 23(8), 1638–1646.
- Pacheco, M. M., and A. Hernandez-Guerra (1999), Seasonal variability of recurrent phytoplankton pigment patterns in the Canary Islands area, *Int. J. Remote Sens.*, 20(7), 1405–1418.
- Paillet, J., and H. Mercier (1997), An inverse model of the eastern North Atlantic general circulation and thermocline ventilation, *Deep Sea Res. Part I*, 44(8), 1293–1328.
- Pelegrí, J., et al. (2005), Hydrographic cruises off northwest Africa: The Canary current and the Cape Ghir region, *J. Mar. Syst.*, 54(1–4), 39–63.
- Peliz, Á., J. Dubert, A. Santos, P. Oliveira, and B. Le Cann (2005), Winter upper ocean circulation in the Western Iberian basin—fronts, Eddies and Poleward Flows: An overview, *Deep Sea Res. Part I*, 52(4), 621–646.
- Peliz, A., J. Dubert, P. Marchesiello, and A. Teles-Machado (2007), Surface circulation in the gulf of cadiz: Model and mean flow structure, *J. Geophys. Res.*, 112, C11015, doi:10.1029/2007JC004159.
- Pérez, F., C. Mouriño, F. Fraga, and A. Ríos (1993), Displacement of water masses and remineralization rates off the Iberian Peninsula by nutrient anomalies, *J. Mar. Res.*, 51(4), 869–892.
- Pérez, F., L. Mintrop, O. Llinas, M. Glez-Davila, C. Castro, M. Alvarez, A. Kortzinger, M. Santana-Casiano, M. Rueda, and A. Rios (2001), Mixing analysis of nutrients, oxygen and inorganic carbon in the Canary Islands region, *J. Mar. Syst.*, 28(3–4), 183–201.
- Pérez, F., M. Gilcoto, and A. Ríos (2003), Large and mesoscale variability of the water masses and the deep chlorophyll maximum in the Azores Front, *J. Geophys. Res.*, 108(C7), 3215, doi:10.1029/2000JV000360.
- Sangrà, P., et al. (2009), The Canary eddy corridor: A major pathway for long-lived eddies in the subtropical North Atlantic, *Deep Sea Res. Part I*, 56(12), 2100–2114.
- Schmitz, W. J. (1996), On the world ocean circulation, volume I, some global features/North Atlantic circulation, *Tech. Rep.*, WHOI-96-03. Funding was provided by the Office of Naval Research, Grant Nos. N00014-89-J-1039 and N00014-95-1-0356, and the Clark Foundation. *Woods Hole Oceanogr. Inst.*
- Siedler, G., L. Armi, and T. Müller (2005), Meddies and decadal changes at the Azores front from 1980 to 2000, *Deep Sea Res. Part II*, 52, 583–604.
- Stramma, L. (1984), Geostrophic transport in the warm water sphere of the eastern subtropical North Atlantic, *J. Mar. Res.*, 42(3), 537–558.
- Stramma, L., and H. Isemer (1988), Seasonal variability of meridional temperature fluxes in the eastern North Atlantic Ocean, *J. Mar. Res.*, 46(2), 281–299.
- Stramma, L., and T. Müller (1989), Some observations of the Azores current and the North Equatorial current, *J. Geophys. Res.*, 94, 3181–3186.
- Stramma, L., and G. Siedler (1988), Seasonal changes in the North Atlantic subtropical gyre, *J. Geophys. Res.*, 93(C7), 8111–8118.
- Tomczak, M., and J. Godfrey (2003), *Regional Oceanography: An Introduction*, Daya Books, Pergamon, U. K.
- Toole, J., and B. Warren (1993), A hydrographic section across the subtropical south Indian Ocean, *Deep Sea Res. Part I*, 40, 1973–2019.
- Tréguer, P., and P. Le Corre (1975), *Manuel d'analyse des sels nutritifs dans leau de mer*, pp. 110, Lab. d'Océanogr. Chim., Univ. de Bretagne Occidentale, Brest.
- Van Aken, H. (2000a), The hydrography of the mid-latitude Northeast Atlantic Ocean I: The deep water masses, *Deep Sea Res. Part I*, 47(5), 757–788.
- Van Aken, H. (2000b), The hydrography of the mid-latitude Northeast Atlantic Ocean II: The intermediate water masses, *Deep Sea Res. Part I*, 47(5), 789–824.
- Volkov, D., and L. Fu (2010), On the reasons for the formation and variability of the Azores current, *J. Phys. Oceanogr.*, 40, 2197–2220, doi:10.1175/2010JPO4326.1.
- Winkler, L. (1888), Die bestimmung des im wasser gelösten sauerstoffes, *Ber. Dtsch. Chem. Ges.*, 21(2), 2843–2854.
- Zimmermann, C., C. Keefe, and N. E. R. L. (US) (1997), *Method 365.5: Determination of Orthophosphate in Estuarine and Coastal Waters by Automated Colorimetric Analysis*, 2nd ed., U.S. EPA, Off. of Res. and Dev., Natl. Exposure Res. Lab, National Exposure Research Laboratory Office of Research and Development U.S. Environmental Protection Agency Cincinnati, Ohio.